Rare Metal Materials and Engineering
Volume 55, Issue 2, February 2026
Available online at www.rmme.ac.cn

Science Press

Cite this article as: Liu Bingxu, You Caiyin, Wang Fenghui, et al. SLM-3D Printed Soft Magnetic Alloys: Process, Performance, and Prospects[J]. Rare Metal Materials and Engineering, 2026, 55(02): 365-388. DOI: https://doi.org/10.12442/j.issn.1002-185X.20250078.

REVIEW

SLM-3D Printed Soft Magnetic Alloys: Process, Performance, and Prospects

Liu Bingxu, You Caiyin, Wang Fenghui, Tian Na, Liu Heguang, Zhang Jing, Zhu Xiaopei

School of Materials Science and Engineering, Xi'an University of Technology, Xi'an 710048, China

Abstract: Soft magnetic alloys are extensively used in various power electronic devices due to their advantageous properties, including high saturation magnetic induction, low coercivity, and high permeability. In certain applications, complex-shaped components are increasingly required for performance enhancement. Additive manufacturing technique, particularly selective laser melting (SLM), has emerged as an effective method for fabricating such complex-shaped soft magnetic components. SLM, a laser-based additive manufacturing technique, employs high-power-density lasers to melt and fuse metal powders within a powder bed selectively. This approach enables rapid prototyping, precise geometrical control, and the integration of multi-material designs. This review highlights recent advancements in the application of SLM technique for the production of soft magnetic alloys, focusing on Fe-Si, Fe-Ni, Fe-Co, and amorphous alloy systems. Moreover, it explores the implementation of SLM in manufacturing processes and evaluates both the opportunities and challenges associated with SLM-based production of soft magnetic alloys.

Key words: additive manufacturing; selective laser melting; soft magnetic alloys; magnetic properties

1 Introduction

Soft magnetic materials, predominantly composed of transition metals (Fe, Co, and Ni) along with their alloys, possess the ability to generate magnetic fields either directly or through induced effects. These properties show great potential of soft magnetic materials in various applications, including motors, mechanical systems, electronic devices, information storage systems, and sensors[1–4]. The rapid advancement of smart technologies, artificial intelligence (AI), 5G communications, biomedical engineering, and aerospace systems proposes increasingly stringent demands on the performance of these materials[5–8]. Among these soft magnetic materials, Fe-based soft magnetic alloys, which are often enhanced with Si, Ni, and/or Co, are characterized by high saturation induction, low coercivity, high permeability, and minimal core loss[9–14]. These properties make them indispensable for the use in electric motors, generators, and transformers, ensuring the superior energy conversion efficiency and supporting the effective energy generation and transmission[15–19].

The diverse applications of soft magnetic alloys across diverse sectors attract much attention[20–21]. Recent researches focus on the miniaturization and complexity of electronic devices. The functional performance of soft magnetic alloys is intricately tied to their geometric and structural characteristics. However, conventional fabrication techniques, including casting[22–27], injection molding[28–31], compaction[32–35], melt spinning[36–38], sintering[39–41], and powder metallurgy[42–44], face restrictions in producing complex-shaped components[45]. These methods also suffer from low material utilization rates, further constraining their efficiency[46]. Consequently, there is a growing interest in innovative fabrication techniques that can enable the creation of complex-shaped soft magnetic devices while enhancing the material utilization rate.

Additive manufacturing (AM), commonly referred to as 3D printing, constructs objects directly from computer-aided design models[47–51]. This technique is capable of producing three-

Received date: February 17, 2025
Foundation item: National Natural Science Foundation of China (52171191, 52371198); Project of Constructing National Independent Innovation Demonstration Zones (XM2024XTGXQ05)
Corresponding author: You Caiyin, Ph. D., Professor, School of Materials Science and Engineering, Xi'an University of Technology, Xi'an 710048, P. R. China, Tel: 0086-29-82312373, E-mail: caiyinyou@xaut.edu.cn

dimensional complex-shaped components, and it is compatible with a wide range of materials, including polymers[52–55], metals[56–60], ceramics[62–65], and composites[66–70]. Unlike traditional manufacturing techniques that rely on molds, AM significantly reduces production time and cost[45]. Moreover, it provides precise control over geometrical configurations and supports multi-material integration, enabling the fabrication of complex structures such as hollow frameworks, lattice designs, and thin-walled components[71–75]. These advantages lead to the widespread adoption of AM in diverse fields, including electronics, robotics, biomedical engineering, energy systems, and environmental applications[76–82]. Consequently, AM is extensively applied across various fields[21], making it a transformative technique with considerable research interest.

AM offers unparalleled design flexibility in the production of soft magnetic alloys, enabling the fabrication of components with complex shape and internal structures[21,83–84]. This capability facilitates the optimization of magnetic flux pathways, enhancing the electromagnetic performance of devices[85–88]. Among various AM techniques, selective laser melting (SLM) stands out as a powder bed fusion method, which employs a focused laser beam to selectively melt and fuse metal powder materials layer-by-layer, enabling the construction of complex parts[89–90]. This approach provides new approach for developing the soft magnetic alloys with enhanced performance and manufacturability[91].

Although extensive researches have been conducted on the application of AM techniques for magnetic material fabrication, comprehensive reviews specifically for SLM technique for producing soft magnetic alloys are rare. This review aims to provide detailed analyses of SLM technique in the manufacture of soft magnetic alloys, which covers the fundamental principles and operation mechanisms. The application of SLM in fabricating various soft magnetic materials was also discussed, including Fe-Si, Fe-Ni, Fe-Co, and amorphous soft magnetic alloys. The process optimization, post-processing methods, and the resultant material properties were displayed. Additionally, the challenges and future directions for the development of SLM technique for soft magnetic alloys were proposed.

2 SLM Fabrication of Soft Magnetic Alloys

2.1 SLM

SLM, also referred to as laser powder bed fusion (L-PBF), is an advanced metal AM technique, which uses a high-energy laser beam to selectively melt metal powder layer-by-layer to produce components with precise geometries. As depicted in Fig.1[93], SLM process involves the application of laser to melt specific regions of metal powder bed based on the geometry of a pre-designed computer-aided design (CAD) model, which sequentially stacks these layers to form a three-dimensional structure. Once the fabrication process is completed, the finished object is removed from the build platform, and the loose unused powder is collected for recycling. SLM

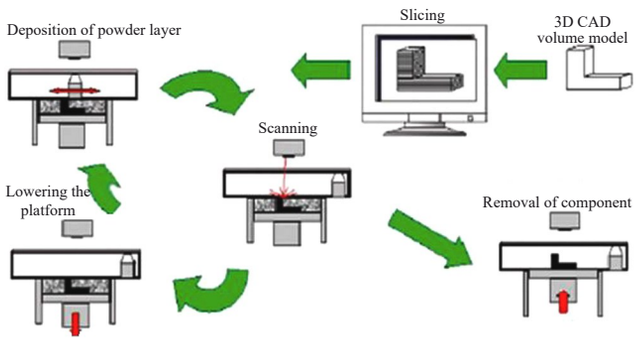

Fig.1 Schematic diagram of SLM process[93]

technique possesses exceptional precision and the ability to produce highly complex-shaped components, which is well-suited for industrial applications with rigorous performance requirements. The process incorporates rapid solidification rates, typically in the range of 10^5–10^6 K/s, which promote the formation of refined grain structures through undercooling, thereby enhancing the mechanical properties of the fabricated components[92]. Despite its advantages, SLM technique faces several challenges. (1) High equipment cost: the machines used for SLM process are expensive, requiring substantial initial investment. (2) Complex post-processing requirements: fabricated components often necessitate the additional steps, such as support removal, heat treatment, and surface finishing, to achieve the desired quality. (3) Quality control issues: the layer-by-layer construction process can introduce defects, such as pores, necessitating rigorous inspection and quality assurance procedures to ensure the consistency and reliability of components.

2.2 Influencing factors of SLM

The fabrication of components with precise and complex shapes using SLM technique for industrial applications requires careful consideration of multiple influencing factors, including raw material properties, process parameters, and post-processing techniques.

2.2.1 Characteristics of raw materials

The particle size and morphology of the powder are pivotal in determining the layer thickness, densification, and flowability of the powder bed[92–100]. Optimal performance can be achieved when the powder exhibits high sphericity and uniform particle size distribution, which enhance the flowability and laser absorption. These are key factors for the improvement of molding quality, mechanical properties, and soft magnetic properties of the fabricated components[101]. Consequently, selecting appropriate raw material powders is fundamental to the production of high-performance soft magnetic alloys via SLM method.

2.2.2 Process parameters

Key process parameters, such as laser power[102], scanning speed, and beam spot diameter, can affect the input energy density during SLM process. The interplay among energy density, microstructure, crystal structure, and soft magnetic properties has been extensively investigated[103–111]. Excessive

energy density can lead to over-melting and pore formation, whereas insufficient energy density can result in inadequate melting and inferior interlayer bonding, both of which may adversely affect the material performance. Furthermore, the adoption of an optimized scanning strategy can mitigate the residual stresses and enhance the quality of fabricated components[112–114]. Thus, investigating the impact of different scanning strategies on soft magnetic alloys is prominent.

Other factors, such as sample geometry, powder layer thickness, ambient atmosphere, and preheat temperature, also play significant roles in SLM manufacturing. Thinner powder layers can improve the density and surface quality of components, albeit the prolonged production time and high cost. An inert atmospheric environment, such as argon or nitrogen, reduces the thermal stresses and oxidation, thereby enhancing the overall properties of materials. Preheating the powder bed or build platform to an appropriate temperature can effectively reduce the residual stresses and minimize the deformation. The optimal preheating temperature is material-dependent and varies based on the specific requirements of the equipment.

2.2.3 Post-treatment process

During SLM process, the material is likely to suffer internal residual stresses due to the rapid cycles of melting and solidification. These stresses can result in deformation or cracking of the part under operational conditions. Heat treatment is a critical technique for mitigating these issues and improving the performance of SLM-manufactured components[115–117]. Annealing, for example, serves to release residual stresses, refine the grain structure, and enhance both the mechanical and soft magnetic properties of the materials. In addition, machining and surface treatments contribute to the improvement of surface quality and dimensional accuracy of the parts, further optimizing the material performance.

2.3 Soft magnetic alloys prepared by SLM

For the soft magnetic alloys prepared by SLM process, the interrelations among machining, post-treatment, microstructure, and material properties are predominantly investigated. The researches about the interrelations of Fe-Si, Fe-Ni, Fe-Co, and amorphous soft magnetic alloys are discussed in this section.

2.3.1 Fe-Si alloy

Fe-Si alloy is characterized by its excellent magnetoelectric properties, ease of mass production, and low cost. It serves as the primary raw material for producing silicon steel (transformer steel and electrical steel), which is widely used in the manufacture of core components for electrical equipment, such as transformers and motors.

The energy density during SLM process plays a critical role in determining the microstructure and properties of soft magnetic alloys. It is found that the high energy density prevents pore formation, while low energy density leads to the development of irregular large pores and unmelted particles within the material[118]. Gao et al[119] fabricated Fe-Si alloy samples with exceptionally low porosity by optimizing the process parameters. With the increase in energy density, porosity was decreased progressively, as illustrated by the microstructures observed by optical microscope (OM), as shown in Fig. 2. After parameter optimization, the microstructure, magnetic properties, and mechanical properties of the samples were evaluated. The samples exhibited a columnar structure with directional growth and <001> texture along the building direction (BD), demonstrating typical soft magnetic behavior with a power loss (P) of 18.8 W/kg at frequency f=50 Hz and magnetic induction intensity B=1 T. ND represents the normal direction. In addition, the samples displayed robust mechanical properties: elongation of 8.8%, ultimate tensile strength of 562 MPa, and yield strength of 445 MPa. Zhong et al[120] used SLM process to fabricate FeSiCr alloys and investigated the influence of the oxide layer thickness on the soft magnetic properties by controlling the oxygen concentration within the chamber at 1000, 4000, and 8000 μL/L. It is found that an oxide layer exists, which results in the reduced core loss and eddy current loss at high frequencies[120], compared with those of conventional silicon steel sheets. Backes et al[121] fabricated Fe-3wt% Si and Fe-9wt% Si alloys using the L-PBF technique with optimized parameters (P=200 W, v=750 mm/s) and various preheating temperatures (200 °C for Fe-3wt% Si and 800 °C for Fe-9wt% Si) to produce minimally-cracked dense samples, as shown in Fig. 3. The results indicated that Fe-9wt% Si exhibited lower magnetic losses, and the magnetic domain structure was influenced by the crystal orientation, as demonstrated in Fig.4. Ji et al[122] employed the design of experiments approach to study the effect of process parameters on the preparation of Fe-4.5wt% Si using SLM method. The optimal parameters were identified through response surface analysis as P=286.36 W and v=1674.24 mm/s. Experimental validation confirmed that these parameters not only yielded the highest relative density but also resulted in the saturation magnetization intensity exceeding the predicted value, and the coercivity is closely matched with the expected outcome. Stella et al[123] performed experimental measurements of the hysteresis loops of Fe-Si alloys fabricated via L-PBF technique. They used artificial neural networks (ANNs) and Jiles-Atherton (JA) model to simulate and predict the loops. The results demonstrated that the hysteresis loops and static power loss densities of Fe-Si alloys could be predicted with greater accuracy using ANNs, outperforming the predictive capabilities of the JA model. Teh et al[124] addressed the restrictions of silicon content in traditional Fe-Si magnetic alloys by fabricating high-density Fe-5Si, Fe-10Si, and Fe-20Si alloys. Their study revealed that these alloys exhibited saturation magnetization values ranging from 0.090 $A\cdot m^2\cdot g^{-1}$ to 0.209 $A\cdot m^2\cdot g^{-1}$, and the coercivity value was between 724.36 and 859.68 $A\cdot m^{-1}$.

Achieving an optimal crystal texture is essential for enhancing the motor efficiency. However, manufacturing stable grain-oriented electrical steel with fewer processing steps remains a challenge. Garibaldi et al[125] employed SLM technique to fabricate high-silicon steel components and

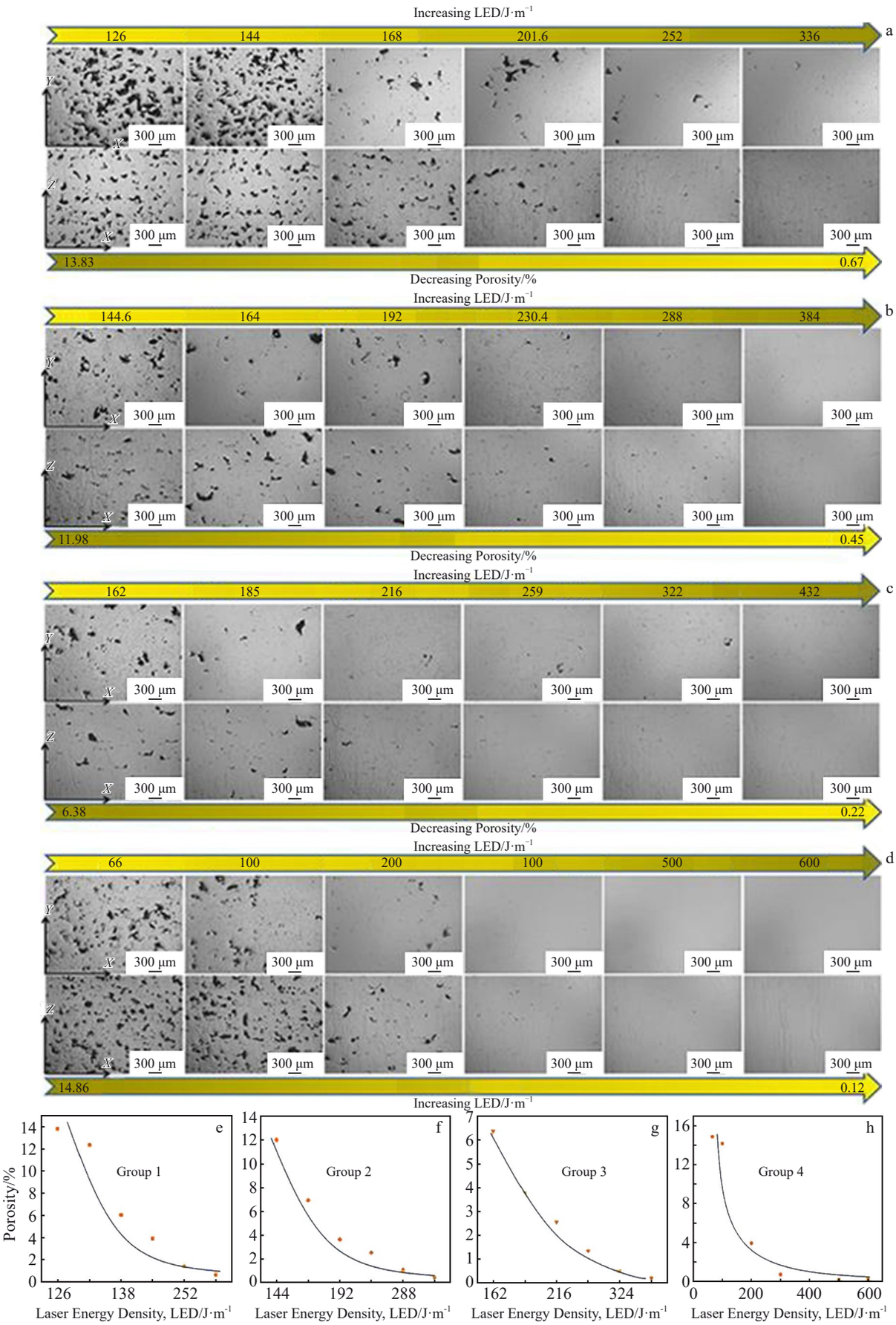

Fig.2 OM images (a–d) and porosity results (e–h) of a series of Fe-Si alloy samples prepared under different energy densities[119]: (a, e) group 1; (b, f) group 2; (c, g) group 3; (d, h) group 4

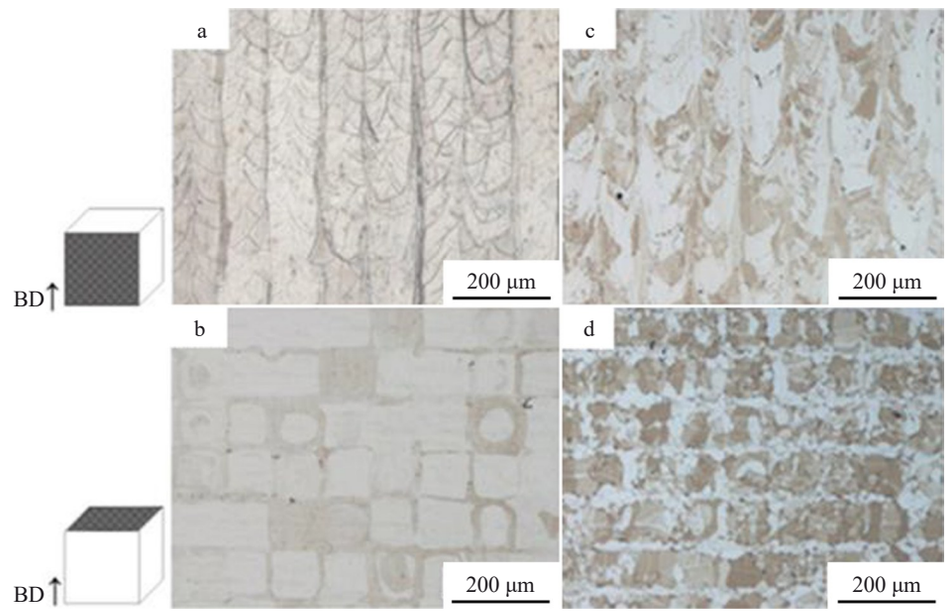

Fig.3 OM images of AM-prepared samples fabricated from powders with 3wt% (a–b) and 9wt% (c–d) Si at platform temperature of 200 °C (a, c) and 800 °C (b, d)[121]

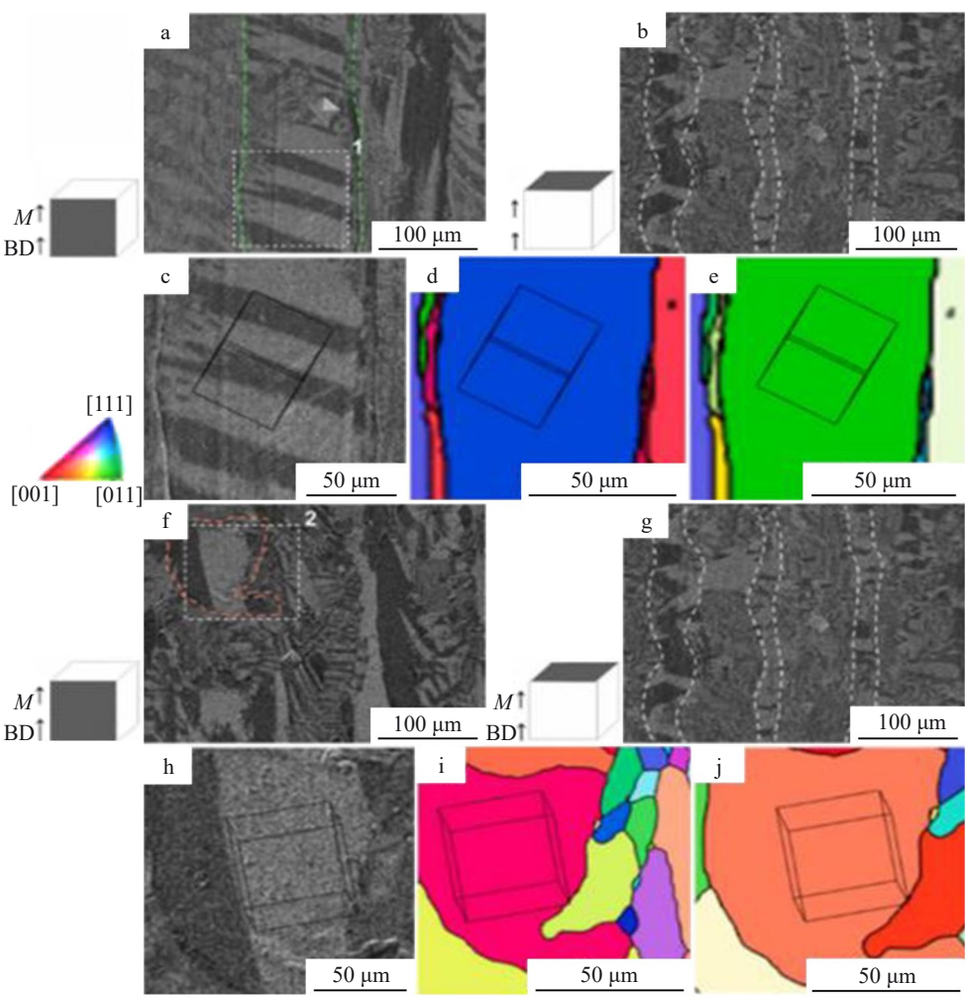

Fig.4 Magnetic domain structures of Fe-3wt% Si sample prepared at 200 °C (a–b) and Fe-9wt% Si sample prepared at 800 °C (f–g); magnified image of area 1 in Fig. 4a (c) and corresponding crystallographic orientations along BD (d) and ND (e); magnified image of area 2 in Fig.4f (h) and corresponding crystallographic orientations along BD (i) and ND (j)[121]

observed that the columnar grains in the as-built samples grew along the BD. With the increase in energy density, the columnar grains are elongated, and the <001> fiber texture was transformed into a cubic texture along BD, as shown in Fig.5. This phenomenon may offer a pathway for the fabrication of three-dimensional grain-oriented high-silicon steels for electro-mechanical applications. They further explored the relationship among laser energy input, microstructure, and magnetic properties[126]. With the increase in energy input, the number of cubic textures was also increased. However, an excessive quantity of cubic textures led to a decline in soft magnetic properties of the material. Samples with a density greater than 99% and a strong crystal texture along BD exhibited the optimal magnetic properties. Therefore, they concluded that the porosity and texture are the primary factors influencing the magnetic properties. To better understand the formation mechanism of the texture, the melt pool shape and boundaries have also been investigated[127]. The melt pool is categorized into three types based on its shape, and different types of melt pool leads to distinct crystal structures, as shown in Fig. 6.

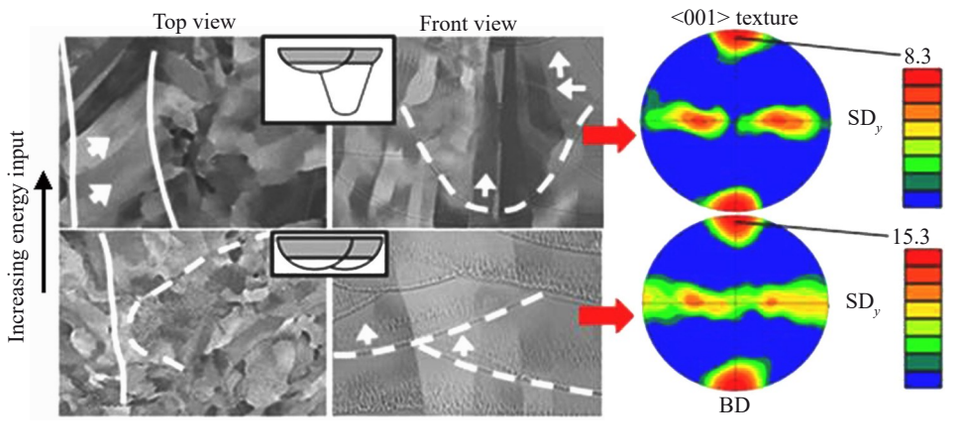

Fig.5 Cross-sectional morphologies and PFs of molten pool under different energy inputs[125]

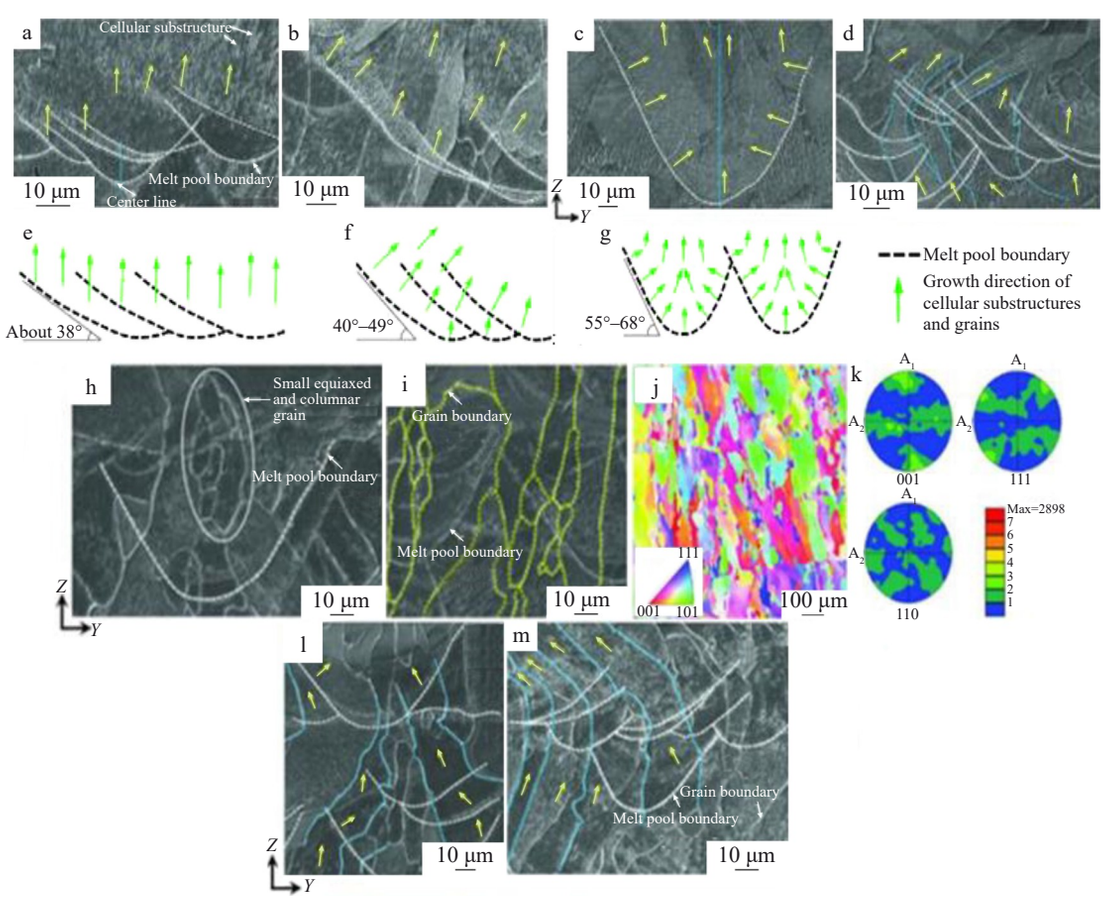

Fig.6 SEM images (a–d) and schematic diagrams (e–g) of shallow melt pool (a–b, e–f), deep melt pool (c, g), and solidification structure showing changes in grain growth direction (d); SEM images (h–i), IPF (j), and PF (k) of cross-section microstructures; SEM images of grain growth direction of deep melt pool (l) and shallow melt pool (m)[127]

Scanning electron microscope (SEM) observation, inverse pole figure (IPF) analysis, pole figure (PF) analysis, and electron backscattered diffraction (EBSD) analysis were conducted. The presence of these three melt pool types caused deviations in the direction of grain growth, ultimately resulting in weaker texture strength.

Beyond process parameters, numerous studies have investigated the relationship between heat treatment and both the microstructural characteristics and the soft magnetic properties of materials[128–130]. After Fe-3wt% Si soft magnets with exceptionally low porosity was prepared, Gao et al[131] examined the impact of heat treatment on the microstructure and magnetic properties of these samples. The microstructure of the as-built samples exhibited columnar crystals with a <001> texture, as shown in Fig.7. After annealing at 1000 °C for 3 h, significant grain growth and stress release can be observed, and the texture is consistent with that of the as-built samples. Additionally, the soft magnetic properties were improved with the increase in annealing temperature and the prolongation of duration. Garibaldi et al[132] also studied the effect of annealing on the microstructure and properties of Fe-Si soft magnetic alloys fabricated by SLM. They found that high-temperature annealing effectively induced stress release and promoted grain growth without compromising the beneficial crystallographic texture. The soft magnetic properties were enhanced, achieving a maximum relative magnetic permeability of 24 000 and a coercivity of 16 A/m, as shown in Fig.8.

The scanning strategy and sample geometry play a critical role in determining the microstructure and properties of Fe-Si alloys. Different scanning strategies, as illustrated in Fig. 9, have been found to influence the microstructure of Fe-Si alloy samples[133]. In comparison to the transverse scanning strategy, which produces very large columnar grains, the longitudinal scanning strategy results in more equiaxed or misoriented grain morphologies with smaller grains. Plotkowski et al[134] demonstrated that texture can be controlled through various

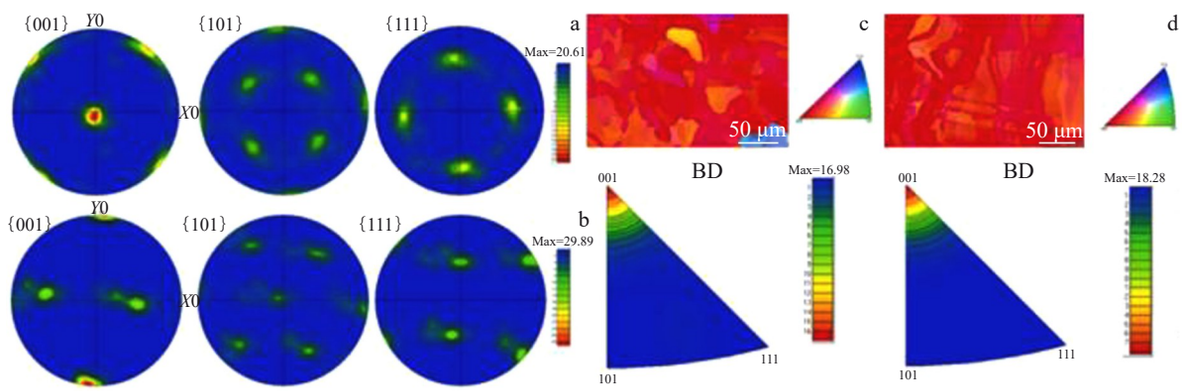

Fig.7 PFs (a–b) and IPFs with EBSD maps (c–d) for *XY* plane (a, c) and *XZ* plane (b, d) of Fe-3wt% Si soft magnets[131]

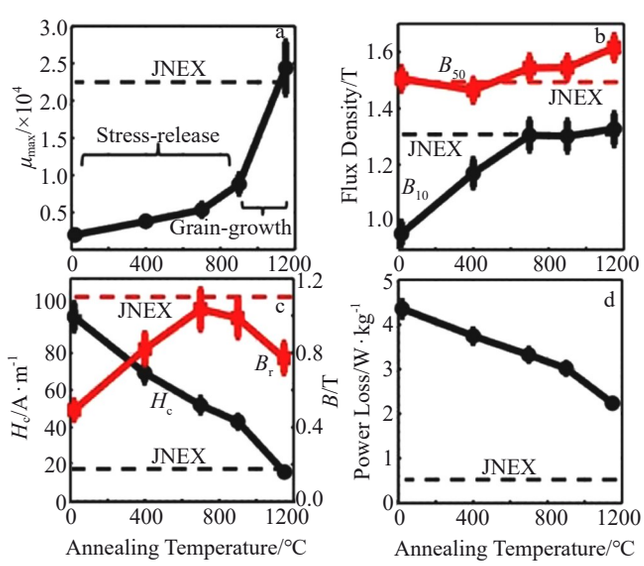

Fig.8 Magnetic properties of SLM-prepared Fe-6.9wt% Si samples at different annealing temperatures[132]: (a) maximum permeability μ_{max}; (b) flux density; (c) coercivity H_c and remanence B_r; (d) power loss at B_{max}=1 T and f=50 Hz

scanning strategies, including single and double scan patterns. The single scan pattern (Fig.10a) produces a chaotic structure with numerous small grains, whereas the double scan pattern (Fig.10b) leads to a distinct orientation of the <100> crystallographic direction along BD, resulting in larger grains growing upward. They also fabricated a series of samples with complex cross-sections (Fig.10c) to investigate their magnetic properties. The findings revealed that geometry has a substantial effect on the magnetic properties, as shown in Fig.10d.

Koo et al[135] introduced a novel AM technique, shell-shaping-selective laser melting (SS-SLM), for fabricating

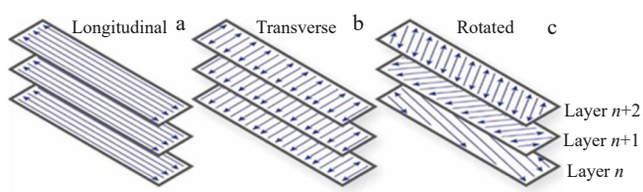

Fig.9 Scan directions relative to the top surface of prism[133]: (a) longitudinal direction, (b) transverses direction, and (c) rotated direction

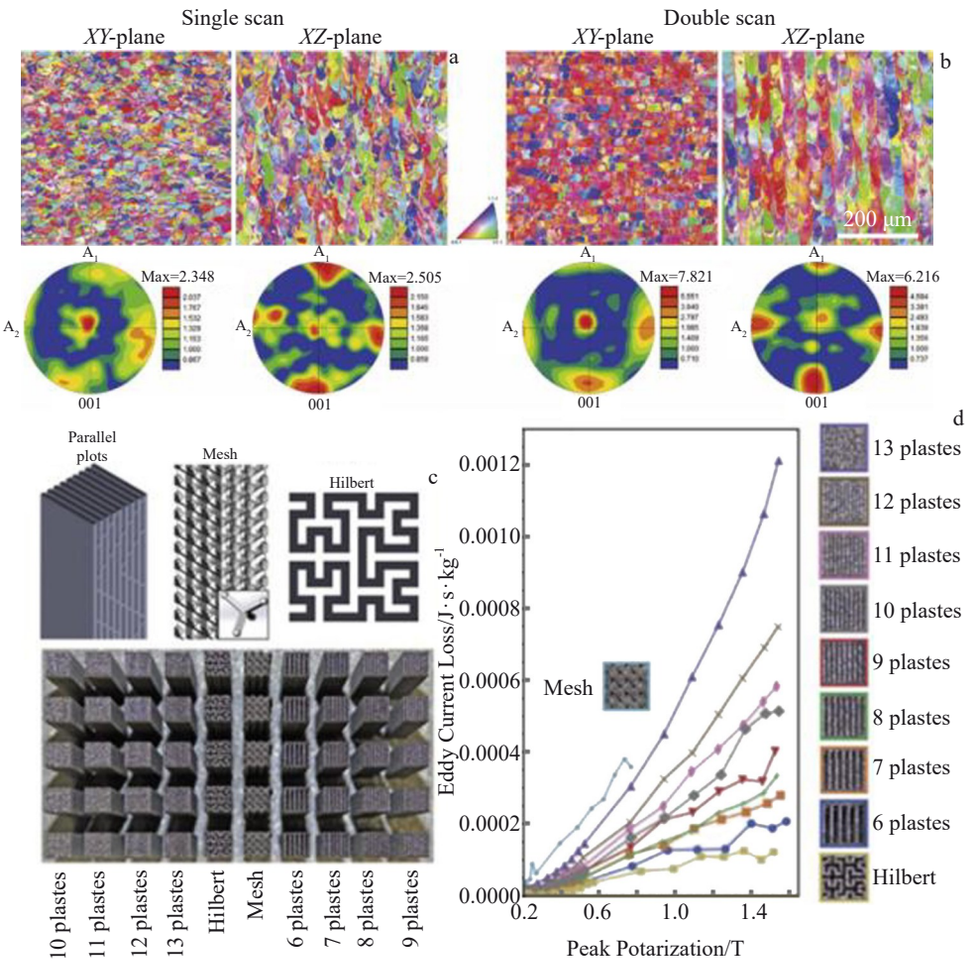

Fig.10 IPFs and PFs of *XY* plane (normal to BD) and *XZ* plane (parallel to BD) under single scan pattern (a) and double scan pattern (b); schematic diagrams of complex cross-section microstructures; eddy current loss coefficients of samples with different geometries (d)[133]

structurally-layered soft magnetic components (SMCs) with a thin surface insulation coating, as depicted in Fig. 11. Schematic diagrams of the integration of an internal insulation layer into SMC are shown in Fig.12. This method enabled the production of high-density Fe-6.5wt% Si SMCs with a relative density of 98%. Subsequent heat treatment induced grain growth, significantly enhancing the soft magnetic properties and achieving coercivity of 34.6 A/m, permeability of 7393, and saturation magnetization of 1.68 T. Moreover, a sol-gel-based process was used to form a uniform and dense insulating layer on the SiO_2 shell, effectively suppressing eddy currents within the shell. Lyrio et al[136] proposed an innovative method for manufacturing thin grain-oriented (GO) electrical steel sheets, employing L-PBF method to fabricate slabs with strong initial textures. These slabs were then subjected to cold rolling and extended annealing to promote abnormal grain growth. This novel process facilitates the production of thin sheets with magnetic properties comparable to that of commercially available GO electrical steels.

Additionally, SLM technique offers the potential to produce

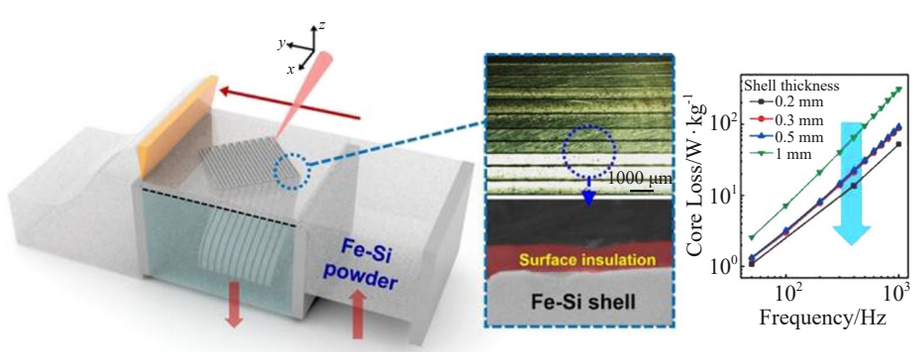

Fig.11 Schematic diagram of SS-SLM process and corresponding eddy current losses for samples with different shell thicknesses[135]

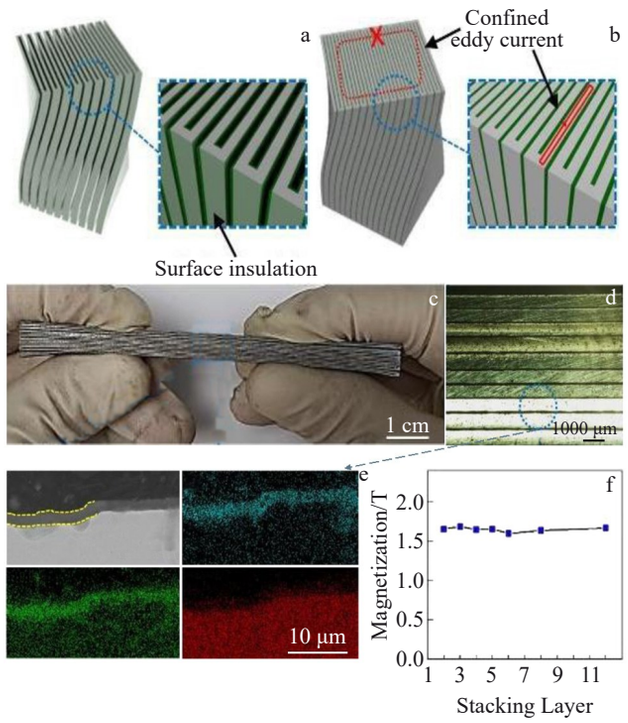

Fig.12 Schematic diagrams of surface insulation formed through sol-gel process (a) and subsequent uniaxial compression (b); appearance of structurally-layered SMCs after insulation and compression (c); cross-section microstructures of SMC and corresponding EDS element mapping results (d–e); saturation magnetization of structurally-layered SMC as a function of the number of stacked shells (f)[135]

iron-silicon alloys with high silicon content. Numerous studies have demonstrated that 6.7wt% Si can significantly enhance the soft magnetic properties of Fe-Si alloys, reducing power loss during the magnetization process[137]. However, increasing silicon content also raises material brittleness, thereby restricting the processibility. Currently, only a few techniques can produce the defect-free Fe-Si alloys with silicon contents of 6.5wt% or higher on an industrial scale. Andreiev et al[129] employed high-temperature powder bed fusion with laser beam (PBF-LB) and a preheating system for the construction chamber to achieve nearly crack-free processing of high-density Fe-Si alloy parts with silicon contents ranging from 2.4wt% to 10.0wt%. This method is suitable for producing large components. As the silicon content increases, hardness improves, but brittleness also rises, and the soft magnetic properties are enhanced. Goll et al[138] fabricated a Fe-6.7wt% Si alloy with high specific resistance (ρ=0.8 μΩ·m) and excellent soft magnetic properties. They also developed a soft magnetic device with a slit-based topological structure, which reduced eddy current losses, as shown in Fig. 13. Additionally, alternating layered structures composed of materials with different resistivity ratios were formed, further reducing eddy current losses, as illustrated in Fig. 14. Macknojia et al[139] prepared Fe-6.5wt% Si alloy samples with a relative density of 99.5% using process parameters of laser power of 180 W, scanning speed of 900 mm/s, hatch spacing of 0.08 mm, and layer thickness of 40 μm. Various core designs with differing cross-sectional areas were fabricated, as shown in Fig. 15. Annealing treatment enhanced the soft magnetic performance of the cores. The core with the smallest cross-sectional area of 3.25 mm^2 exhibited the optimal comprehensive soft magnetic properties.

In addition to their soft magnetic properties, the mechanical characteristics of Fe-Si alloys fabricated via SLM have attracted significant attention. Alleg et al[140] used SLM technique to fabricate FeSiB alloys, achieving high density, low surface roughness, and impressive microhardness values ranging from 1654 HV to 2273 HV, alongside excellent soft magnetic performance. Similarly, Gao et al[119] produced Fe-3wt% Si soft magnets with exceptionally low porosity using SLM technique, which demonstrated remarkable mechanical

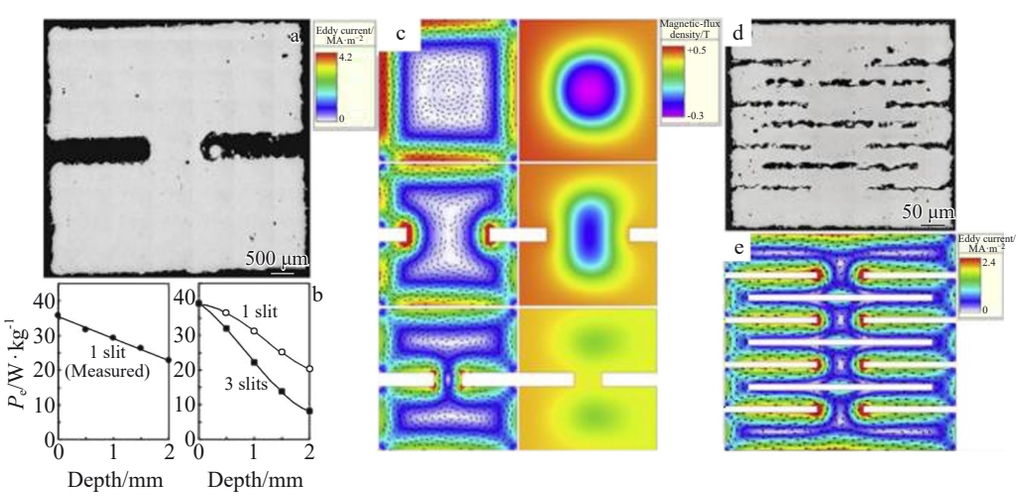

Fig.13 Cross-sectional view of ring (a); experiment and simulation results of eddy current losses as a function of slit depth (b); finite element simulations of eddy current and magnetic flux density with different slit depths (c); cross-sectional view of ring with a more complex topological structure (d); finite element simulation result of eddy current in more complicated structural ring (e)[138]

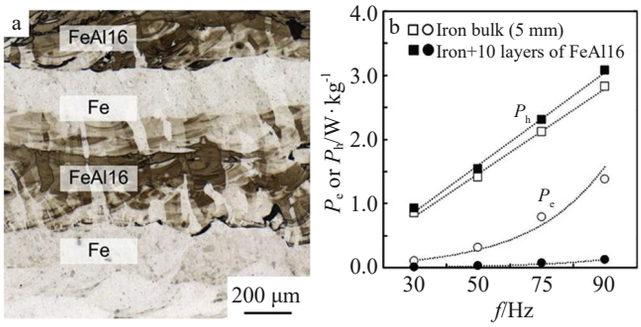

Fig.14 OM cross-section microstructure of multi-layered structure (a); comparison of hysteresis loss (P_h) and eddy current loss (P_e) curves of iron materials with multi-layered structure and bulk structure (b)[138]

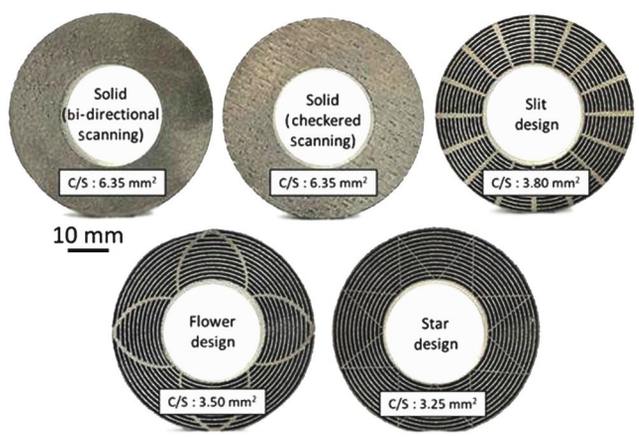

Fig.15 L-PBF-manufactured Fe-6.5wt% Si cores with different design configurations[139]

properties, including microhardness of 235 $HV_{0.1}$, elongation of 8.8%, ultimate tensile strength of 562 MPa, and yield strength of 445 MPa. Additionally, their wear and fracture mechanisms were thoroughly analyzed, as depicted in Fig. 16. The primary fracture mode was identified as a mixed ductile-brittle failure, while adhesive and abrasive wear mechanisms dominated the wear behavior.

2.3.2 Fe-Ni alloy

The Fe-Ni alloys with Ni content ranging from 30wt% to 90wt% are commonly referred to as permalloy. Permalloy is known for its high plasticity. It can be cold-rolled into ultra-thin strips with thickness of as thin as 1 μm. As a soft magnetic material with high permeability and low coercivity in weak magnetic fields, Fe-Ni alloys are widely used in industrial applications. However, conventional processing methods for Fe-Ni alloy fabrication face challenges in producing complexly shaped components and achieving optimal magnetic properties due to the work-hardening effects of the nickel element. Recently, laser-based fabrication techniques, such as SLM, have garnered considerable attention for processing Fe-Ni alloys.

Researchers have investigated the relationship between microstructure and magnetic properties during the laser melting process of Fe-Ni alloys. Kang et al[141] used nickel-

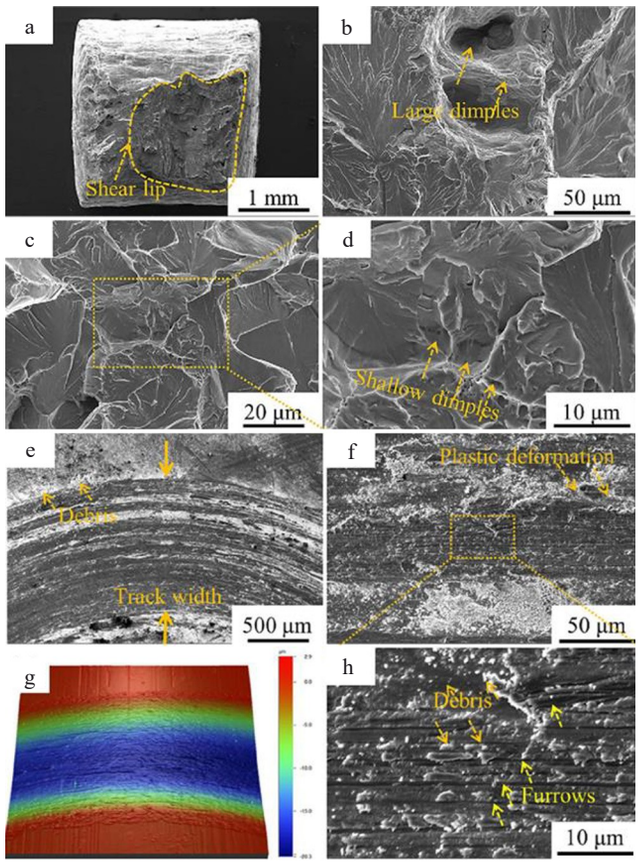

Fig.16 SEM images of fracture morphologies of SLM-prepared Fe-3wt% Si part (a – d); worn surface morphologies of SLM-prepared wear part (e–h)[119]

plated high-silicon steel powder as a raw material to fabricate Fe-Ni-Si soft magnetic alloys using SLM technique. As the laser scanning speed decreased, pores were nearly eliminated. However, cracks appeared, as shown in Fig. 17. Conversely, increasing the laser scanning speed leads to a gradual

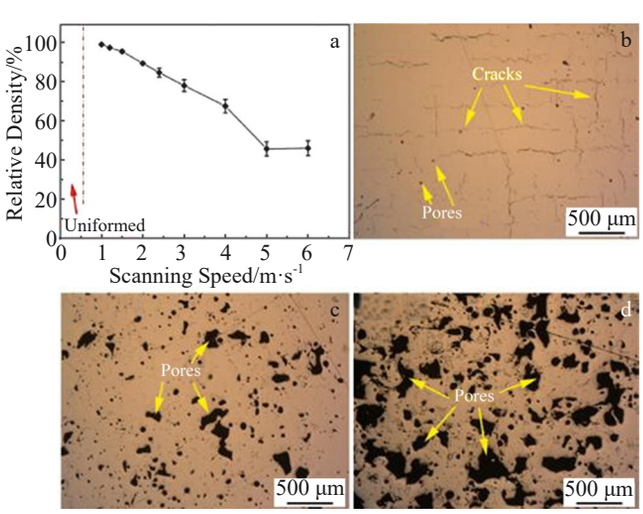

Fig.17 Relative density of SLM-processed Fe-Ni-Si alloys (a); defect morphologies of SLM-processed samples at laser scanning speeds of 1 m/s (b), 2 m/s (c), and 4 m/s (d)[141]

reduction in saturation magnetization, which is related to microstructural variations, such as pores and melt pool formation. Mandal et al[142] found that the laser power density of 1 J/mm^2 was optimal for producing fully dense Fe-Ni alloys using powders milled from 12 h to 24 h. Under these conditions, the thickness of the melt pool was influenced by the particle size and uniformity of the powder, as illustrated in Fig. 18. The alloy elements in the laser-melted sample were evenly distributed with no noticeable segregation, as shown in Fig. 18c. Laser melting can enhance the soft magnetic properties of Fe-Ni alloys, and the microstructure and crystallographic orientation play a pivotal role in these properties. Zhang et al[143] characterized the microstructures of Fe-Ni alloys processed under various laser parameters and assessed the magnetic properties of the resulting samples. The results revealed that SLM-prepared Fe-30% Ni alloy exhibited low coercivity and high saturation magnetization, and its magnetic behavior was strongly influenced by the laser parameters. Moreover, it was demonstrated that SLM-prepared Fe-80% Ni alloy could achieve relatively low coercivity (2338–3184 A/m) and high saturation magnetization (0.08–0.10 A·m^2·g^{-1}) when the optimized laser parameters were used[144]. Shishkovsky et al[145] examined the microstructures of Fe-80% Ni alloy samples in relation to the laser processing parameters and evaluated the influence of external magnetic fields (EMFs) on the growth of microstructures during laser melting. They found that a reduction in coherent-scattering regions of magnetic phases under SLM with the presence of EMF corresponding to the increase in coercivity.

The performance of Fe-Ni alloy samples with complex geometries has also been investigated. Liu et al[146] fabricated Fe-Ni alloy magnetic cores with intricate structures using SLM technique, as shown in Fig. 19. Their study revealed that the maximum magnetization, initial permeability, and coercivity were 0.151 A·m^2·g^{-1}, 310, and 549.24 A/m, respectively. Furthermore, sandblasting followed by annealing at

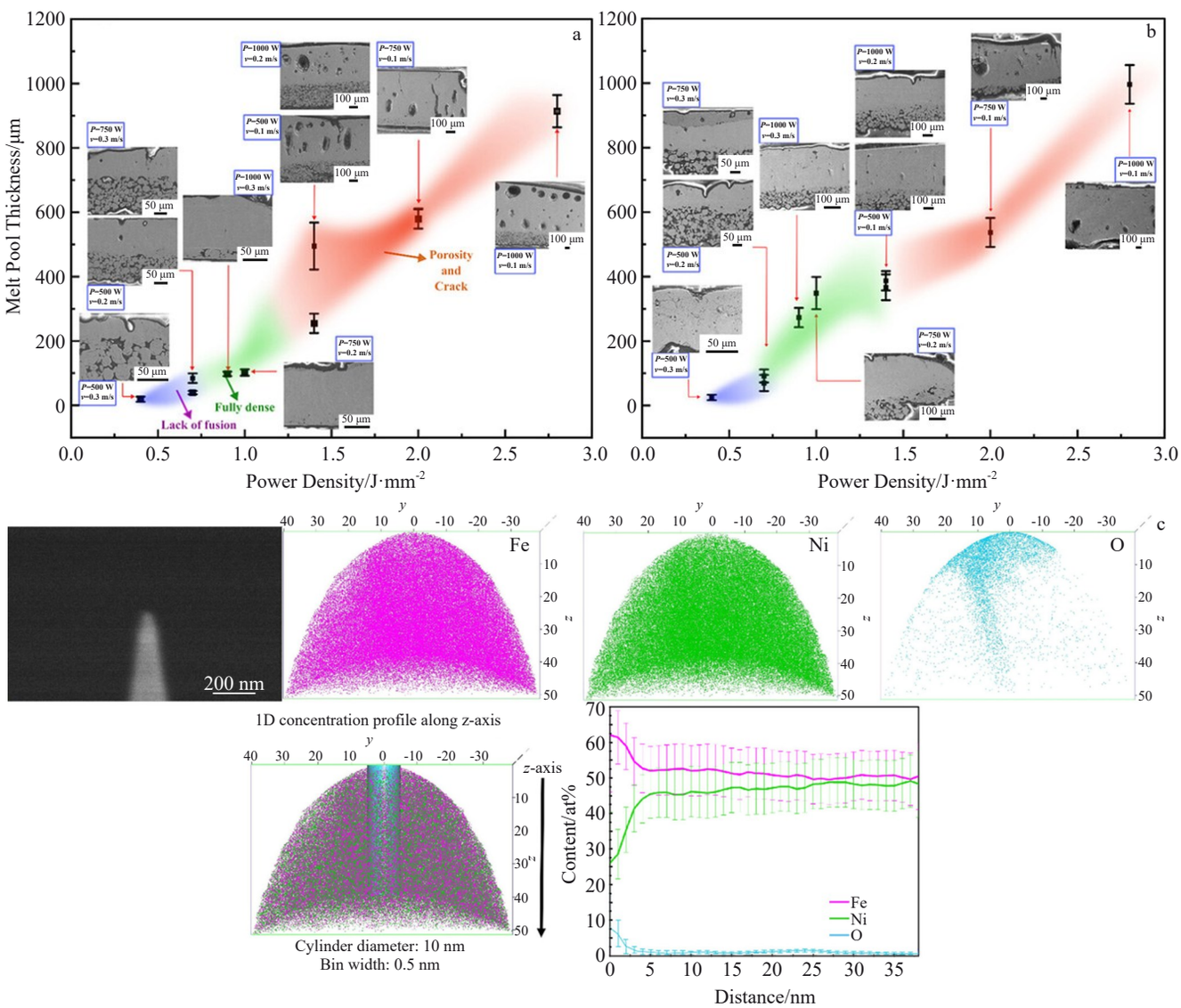

Fig.18 Correlations between laser power density and microstructure of melt pool cross-section of samples prepared by Fe-Ni powders milled for 12 h (a) and 24 h (b); atomic probe tomography image, element distribution maps, and element distribution analyses of sample (c)[142]

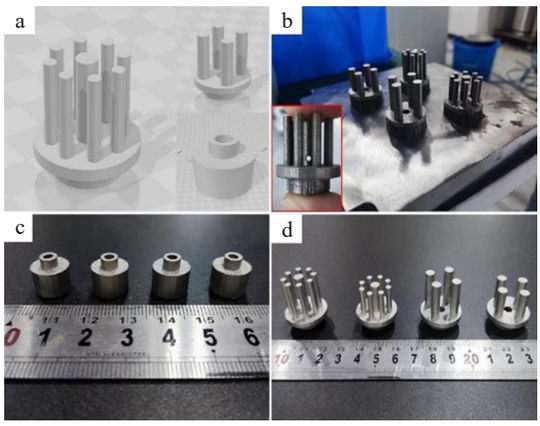

Fig.19 Components with complex geometries[146]: (a) CAD model; (b) SLM-manufactured magnetic cores before sandblasting; (c) SLM-manufactured bases (supporting magnetic sensors) after sandblasting: (d) SLM-manufactured magnetic cores after sandblasting

1300 °C resulted in a remarkable tensile strength of approximately 1060 MPa, along with excellent overall mechanical properties. Additionally, controlling the grain orientation during the laser powder bed melting process was also investigated[147]. By controlling BD during manufacturing, they were able to control the primary texture in the sample, leading to enhanced magnetic properties of the soft magnet, as illustrated in Fig.20.

The influence of heat treatment on the properties of Fe-Ni alloys produced by SLM has also garnered attention. Mazeeva et al[85] investigated the properties of Fe-50% Ni soft magnetic alloys as a function of heat treatment parameters, including temperature and holding time. After annealing, the microhardness decreased from 275 HV to 190 HV, while the relative maximum magnetic permeability increased from 1000 to 5000, and the coercive force decreased to 100 A/m, as shown in Fig.21. Lv et al[116] identified a set of optimal SLM processing parameters that achieved high packing density and exceptionally low surface roughness for the samples.

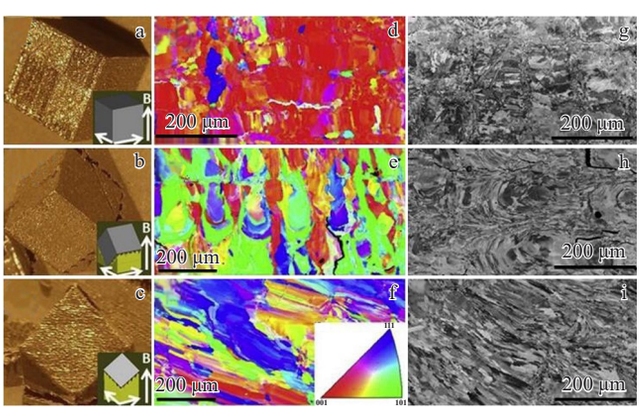

Fig.20 Appearances (a–c), EBSD maps (d–f), and SEM images (g–i) of permalloy-80 of different orientations[147]: (a, d, g) <100> orientation; (b, e, h) <110> orientation; (c, f, i) <111> orientation

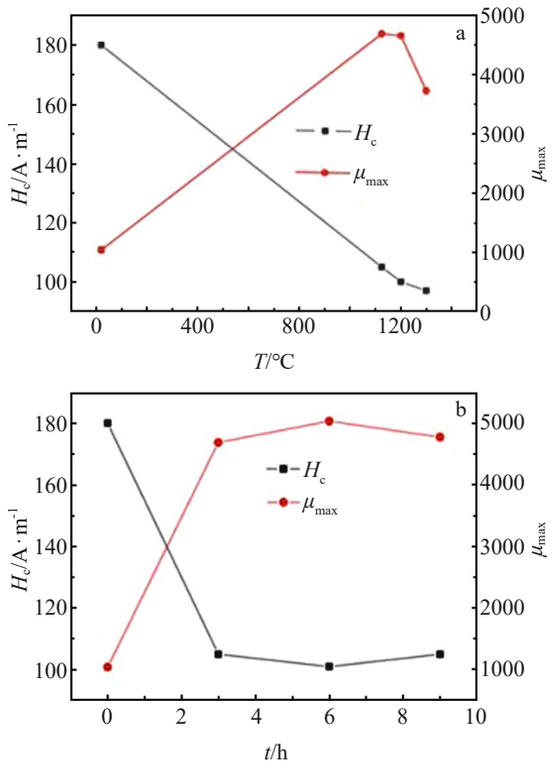

Fig.21 Relationships of relative maximum magnetic permeability and coercivity with heat treatment temperature (a); relationship between heat treatment holding time and magnetic properties (b)[85]

Furthermore, the annealed Ni-15Fe-5Mo alloy exhibited anisotropic behavior in terms of its microstructure, mechanical properties, and magnetic properties. The saturation magnetization of the alloy after SLM processing and subsequent annealing was 0.078 A·m^2·g^{-1}, which was comparable to that of conventionally processed parts.

2.3.3 Fe-Co alloy

The cobalt content in Fe-Co alloys typically ranges from 27wt% to 51wt%, imparting the saturation magnetization. For instance, the saturation magnetization of 35Co-Fe alloy reaches 2.43 T, which is higher than that of pure electromagnetic iron by 13%. However, binary Fe-Co alloys suffer from inferior mechanical properties, particularly low electrical resistivity. Appropriate addition of chromium (Cr) and vanadium (V) can improve both the processing performance and ductility of the alloy while maintaining favorable magnetic properties. These alloys are particularly suited for applications requiring high saturation magnetization and superior soft magnetic properties, such as motor rotors, stators, and transformers. SLM technique offers opportunities to optimize the shape, material composition, volume, and quality of magnetic cores, positioning it as a promising method for fabricating Fe-Co alloys.

In response to the challenge of inferior mechanical properties of binary Fe-Co alloys, researchers use SLM technique to enhance their ductility and overall mechanical

performance. Babuska et al[148] used L-PBF process to fabricate Fe-Co alloys without macroscopic defects, which exhibited both high tensile strength (600 – 700 MPa) and significant ductility (35%). Compared with the traditional forged materials, these alloys demonstrated a significant increase in strength by 300% and an order-of-magnitude improvement in ductility, as shown in Fig. 22. Additionally, they employed a novel design of heat sink for AM process of metal materials, achieving a low-strength and low-ductility Fe-Co alloy, as illustrated in Fig. 23. Li et al[150] applied L-PBF technique to produce block-like Fe-Co alloys with a microstructure predominantly consisting of disordered body-centered cubic (bcc) phases, which exhibited significant ductility. Selected area electron diffraction (SAED) pattern was used to analyze phase content. Subsequent annealing heat treatment facilitated the phase transition from disordered bcc phase to ordered B2 phase, as shown in Fig. 24. This process reduced dislocation density and residual stress, enhancing the soft magnetic properties of the material. The resulting magnetic properties were comparable to those of Fe-Co alloys produced by conventional methods, as shown in Fig. 25. This study presents a novel approach for the one-step manufacturing of net-formed block-shaped Fe-Co alloys with complex geometries.

Researchers have also focused on optimization of process parameters to obtain low-porosity crack-free samples, and they have explored the effects of heat treatment[150] on the structure and properties of these alloys. Riipinen et al[151] investigated the L-PBF fabrication of Fe-49Co-2V alloy. The optimal conditions were identified as laser power of 200 W, scanning speed of 775 mm/s, and hatch distance of 80 μm. Under these parameters, the sample exhibited minimal porosity (0.07%). Subsequently, a series of heat treatments was performed. The annealing at 820 °C for 10 h resulted in the optimal magnetic properties and a uniform microstructure composed of large grains. It was found that a homogeneous microstructure with larger grains is essential for achieving low coercivity and high permeability[152]. Liogas et al[153] examined the impact of heat treatment on the microstructure, structural order, and soft magnetic properties of Fe-Co alloys. Optimal processing parameters for producing low-porosity crack-free samples were determined, as shown in Fig. 26. After heat treatment, the samples underwent recrystallization, and under HT6 conditions, the grains were primarily equiaxed with an average size of 61 μm, as shown in Fig. 27, displaying a fully ordered B2 phase (Fig. 28). The quasistatic soft magnetic properties were superior to those of commercial Co-Fe alloys: the maximum relative permeability exceeded 8000, coercivity

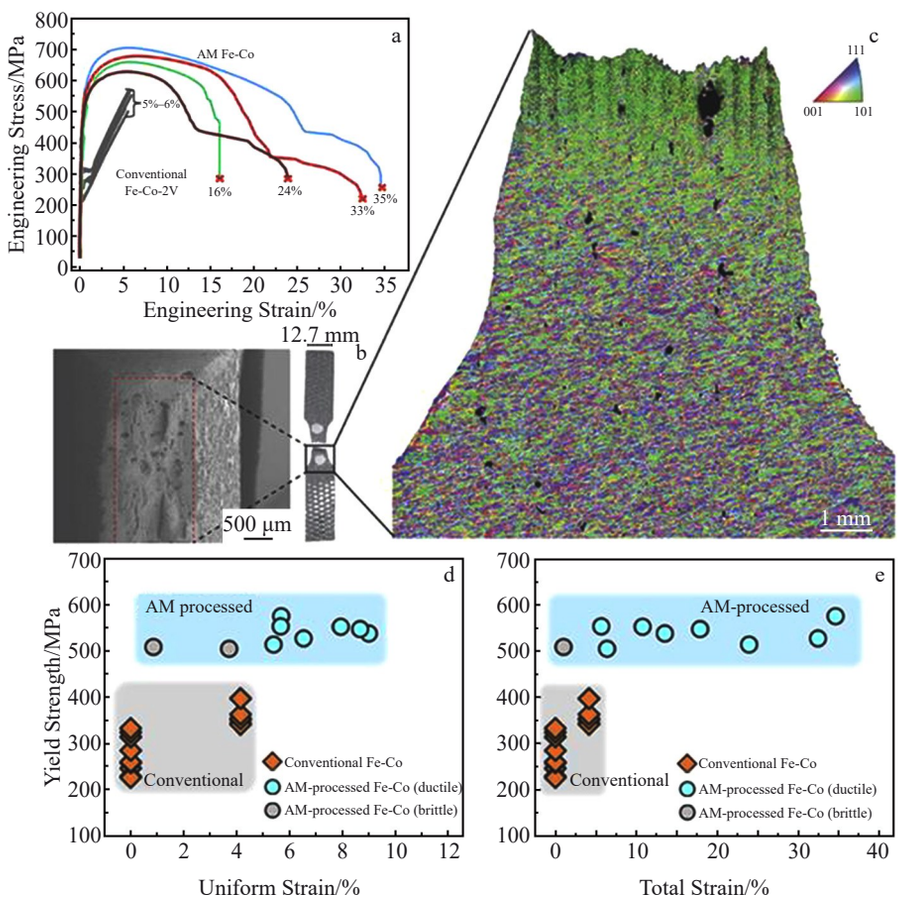

Fig.22 Engineering stress-engineering strain curves of Fe-Co series alloys (a); SEM image (b) and corresponding EBSD mapping (c) of Fe-Co alloy after fracture; yield strength results as a function of uniform strain (d) and total strain (e) for conventionally processed and AM-processed binary Fe-Co alloys[148]

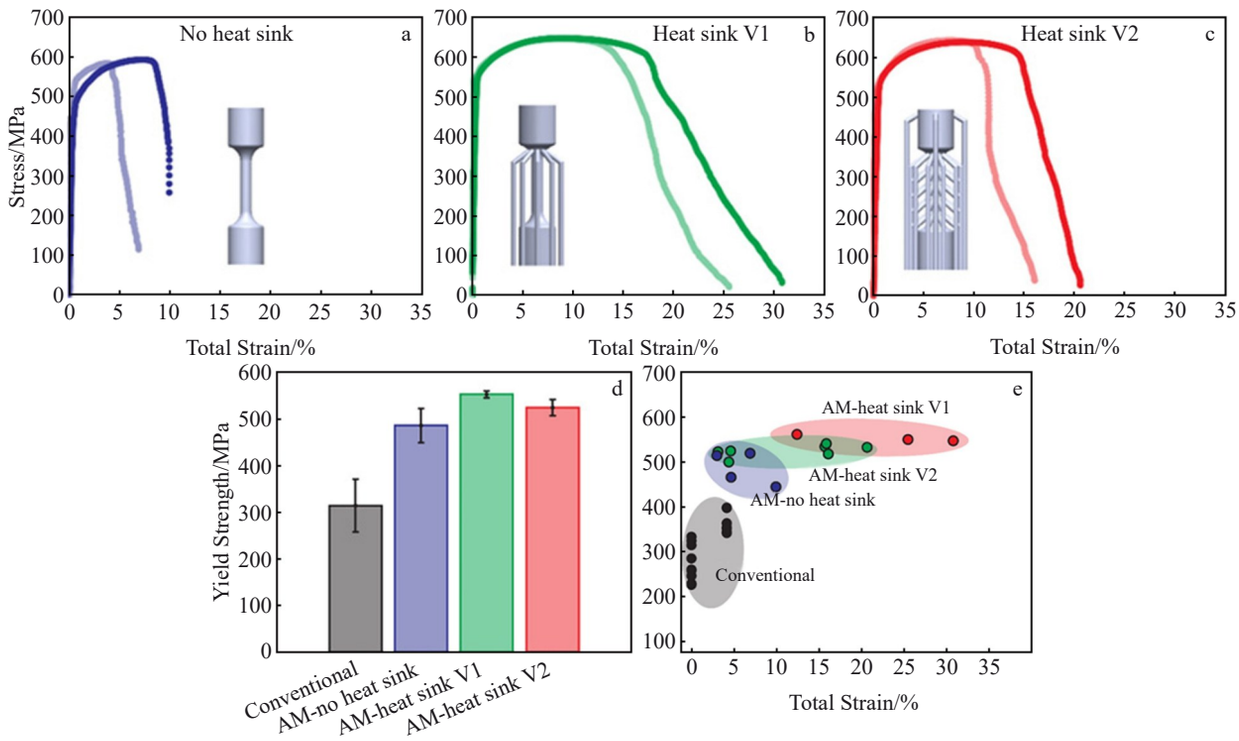

Fig.23 Relationships between tensile stress and total strain of AM-processed Fe-Co alloys prepared without (a) and with heat sinks (b–c); comparison of yield strength of different Fe-Co alloys (d); relationship between yield strength and total strain of different Fe-Co alloys[149]

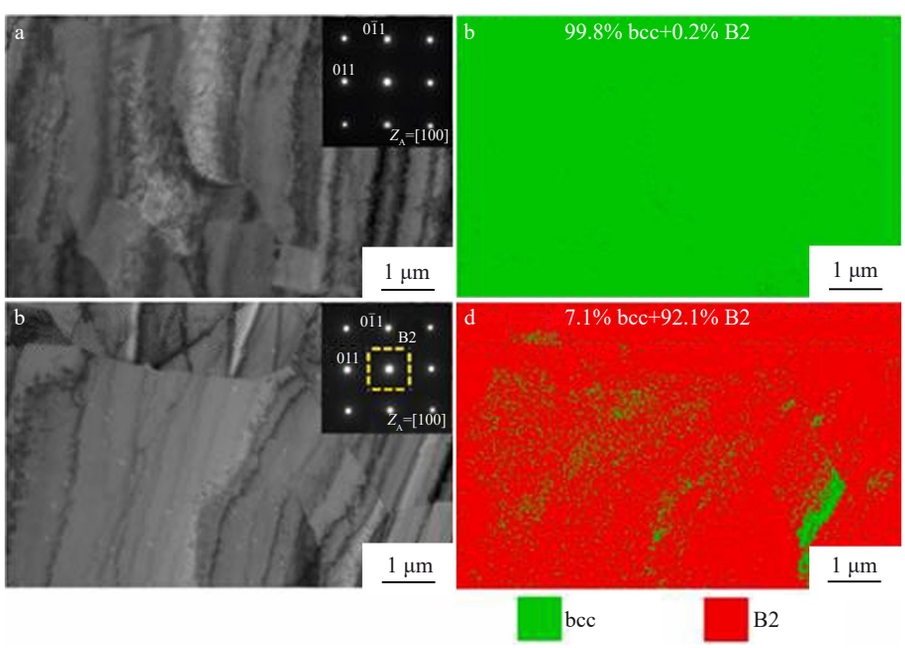

Fig.24 TEM images with SAED patterns (a, c) and corresponding phase mappings (b, d) of as-fabricated (a–b) and heat-treated (c–d) Fe-Co alloys[150]

was as low as 112 A/m, and the magnetic saturation polarization was 2.39 T. Lindroos et al[154] optimized the process parameters for Fe-Co-based alloys and studied the effect of heat treatment on the magnetic properties of materials. The study demonstrated that under optimal heat treatment conditions, the magnetic properties of the samples were comparable to those of commercial Fe-49Co-2V alloys. Additionally, by refining the sample structure, the eddy current losses of the material were significantly reduced, as illustrated in Fig.29.

Everhart et al[155] explored the impact of grain size on the mechanical and soft magnetic properties of Fe-Co-2V alloys

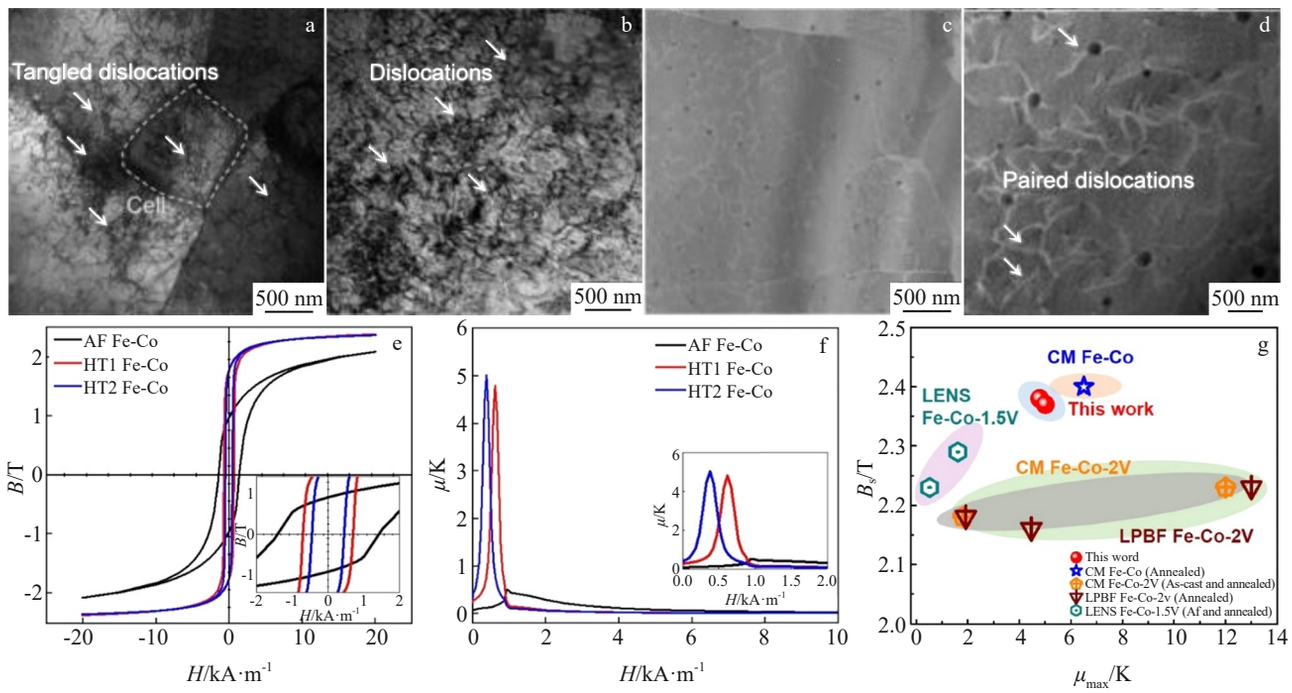

Fig.25 Representative TEM images of as-fabricated (a–b) and heat-treated (c–d) Fe-Co alloys before (a, c) and after (b, d) tensile test; magnetic properties of as-fabricated and heat-treated Fe-Co alloys (e–g)[150]

fabricated via SLM. Their findings indicated that SLM-fabricated materials exhibit excellent mechanical properties, which are comparable to those of conventionally forged materials in the quenched state. The ductility exceeds 20%. Furthermore, the yield strength of SLM-processed materials is influenced by the Hall-Petch effect. However, the relationship between magnetization and grain size deviates from expected trends. Although additional research is required to fully understand the underlying mechanisms driving these trends, the behavior of Fe-Co-2V alloys produced by SLM is largely consistent with that of traditionally forged materials. Future work should focus on optimizing heat treatment processes to enhance the soft magnetic properties. Nonetheless, it is anticipated that SLM-fabricated Fe-Co-2V alloys can be effectively used in magnetic applications.

2.3.4 Amorphous soft magnetic alloys

Amorphous soft magnetic alloys, also referred to as metallic glasses, are materials characterized by their unique disordered atomic structure, resembling a glassy state, in contrast to the crystalline structure of conventional metals. These alloys can be broadly classified into two categories: metal-metal type and metal-metalloid type. The metal-metal type alloys, such as Fe-based, Ni-based, and Co-based alloys, are particularly prevalent. Recent research on the preparation of amorphous soft magnetic alloys using SLM technique has gained significant attention, particularly for the Fe-based amorphous alloys.

Fe-based amorphous soft magnetic alloys are primarily composed of iron and typically fabricated by rapidly cooling the molten alloy to achieve a disordered structure. These alloys offer several key advantages, including low hysteresis loss, low coercivity, high magnetic permeability, and high resistivity, making them ideal for efficient operation in low magnetic fields and high-frequency applications. Additionally, these materials demonstrate favorable mechanical properties, corrosion resistance, and cost-effectiveness, leading to their widespread use in power electronics, transformers, and high-frequency devices. Gao et al[156] used SLM technique to fabricate an amorphous FeSiBCrC composite alloy, which is different from conventional SLM FeSi alloys, typically exhibiting a columnar structure along BD. The inclusion of hard amorphous FeB and Fe_2B phases in the alloy resulted in a microhardness beyond 900 $HV_{0.1}$. Moreover, the SLM alloy demonstrated consistent coercivity (nearly 6288.4 A/m) and high saturation magnetization (0.162 $A \cdot m^2 \cdot g^{-1}$) in both the X and Z directions, as shown in Fig. 30. Additionally, Sufiiarov et al[157] investigated the structure, mechanical properties, and magnetic characteristics of Fe-Si-B alloys produced by SLM process. After optimizing SLM process, a crack-free sample was prepared, and the presence of an amorphous phase was confirmed. Furthermore, annealed samples containing the amorphous phase exhibited enhanced soft magnetic properties.

The impact of process parameters on sample properties during manufacturing has attracted considerable attention. Jung et al[158] examined the effects of scanning speed (v) and laser power (P) on the structure and properties of Fe-based amorphous soft magnetic alloys. As shown in Fig. 31, under low scanning speed and high laser power conditions, the samples exhibited a relative density of 99.7%. Structural and calorimetric analyses indicated that SLM samples were entirely amorphous, exhibiting crystallization behavior and intrinsic magnetic properties which are nearly identical to

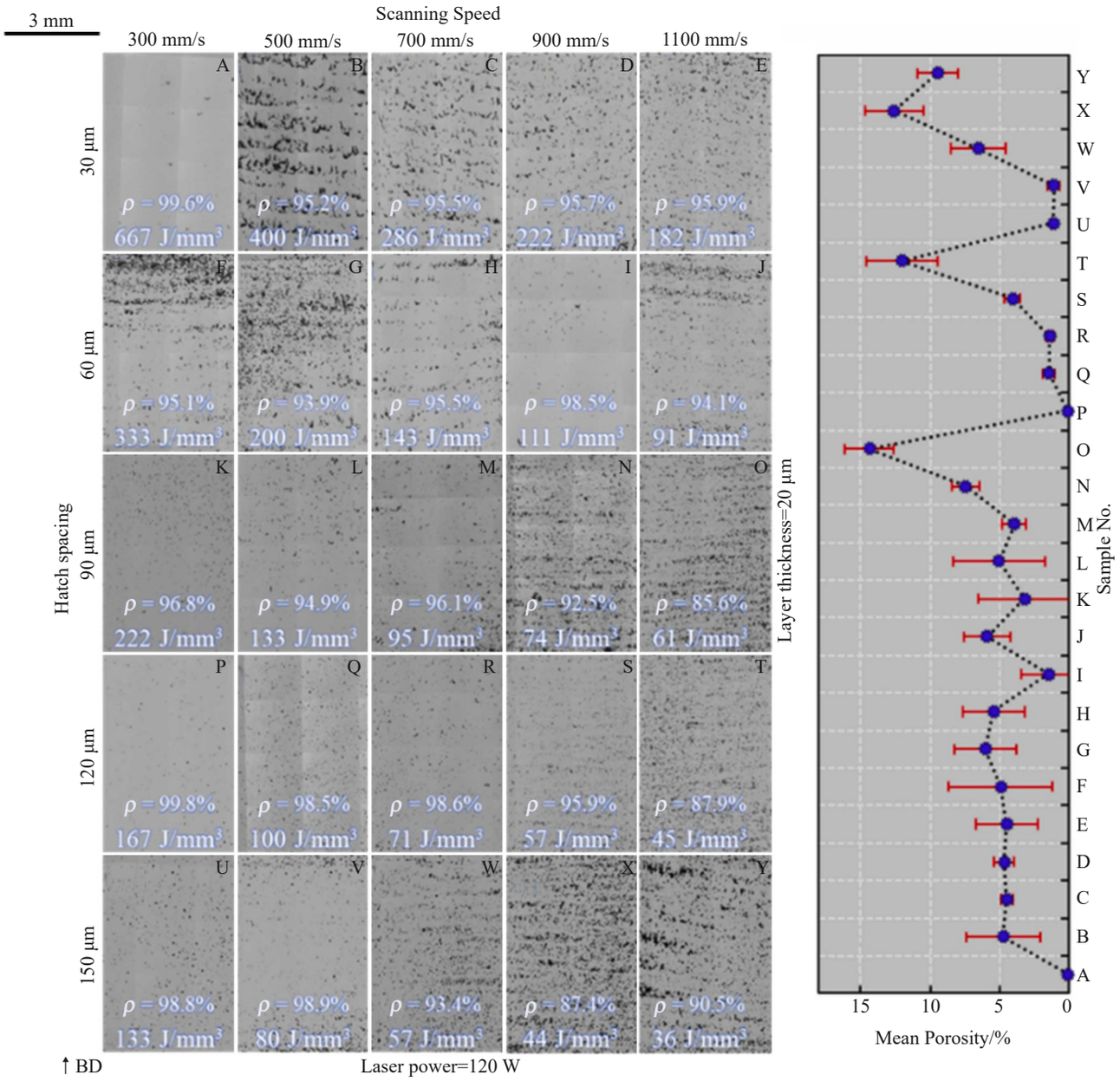

Fig.26 Influence of L-PBF process parameters on the consolidation behavior of Co-Fe alloys[153]

those of the original gas-atomized powder. However, as depicted in Fig. 32, a slight decrease in saturation magnetization and coercivity was noted after SLM, which was likely due to the presence of micropores and cracks in the samples. Özden et al[159] explored the influence of optimizing L-PBF process on the bulk density and soft magnetic properties of FeSiBCrC amorphous alloys. This study focused on various process parameters, including laser power (*P*), scanning speed (*v*), hatch distance (*h*), and layer thickness (*t*). The findings revealed that reducing laser power and increasing scanning speed promoted the formation of the amorphous phase, improving the soft magnetic properties of materials. Additionally, hatch distance could influence the solidification rate, which in turn affected the grain size. Excessive layer thickness, however, led to increased internal thermal stress, causing cracks and pores, which ultimately reduced both density and soft magnetic properties. Rodríguez-Sánchez et al[160] further investigated the relationship between L-PBF process parameters and structural and magnetic characteristics of the materials. Maurya et al[161] performed an in-depth microstructural analysis of titanium carbide iron-based ceramic materials (TiC-Fe) fabricated via SLM. Their study demonstrated that higher scanning speeds resulted in finer grain structures, higher dislocation density, and elevated residual stresses, which collectively contributed to a reduction in ductility.

The influence of scanning strategies on the properties of samples during 3D printing process has received significant research attention. The dual scanning strategy involves re-scanning of the material with laser under consistent power and

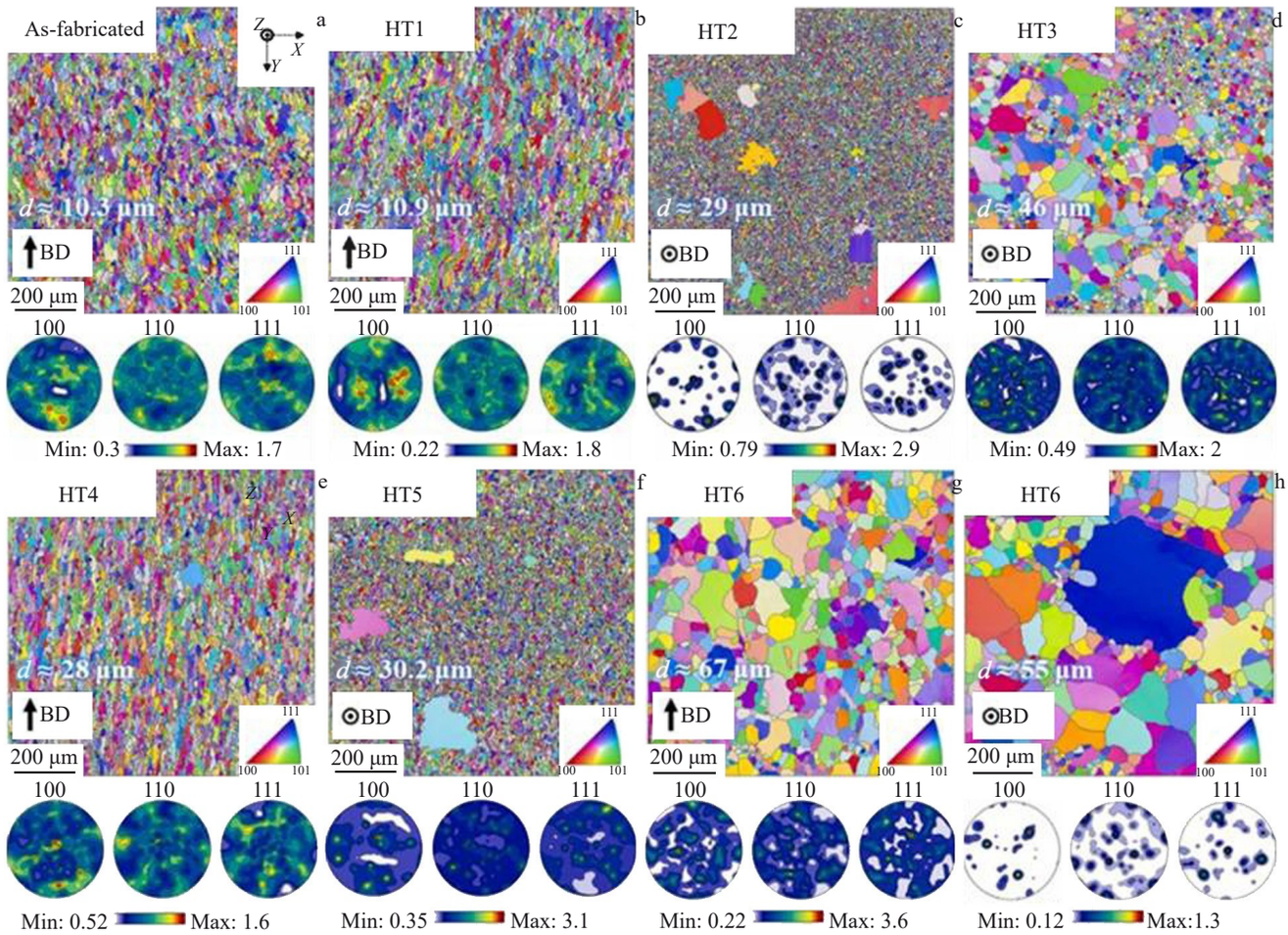

Fig.27 EBSD maps and PFs of as-fabricated and heat-treated Fe-Co alloys[153]

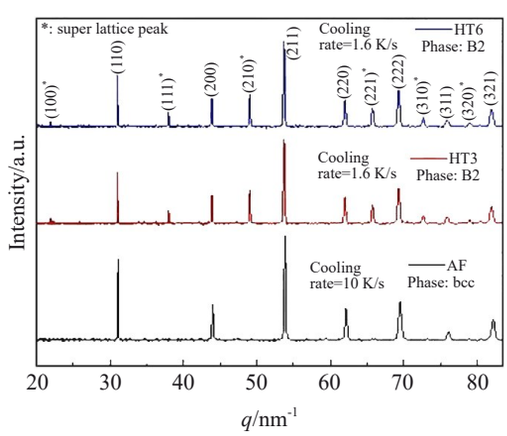

Fig.28 Neutron diffraction patterns of as-fabricated and heat-treated samples[153]

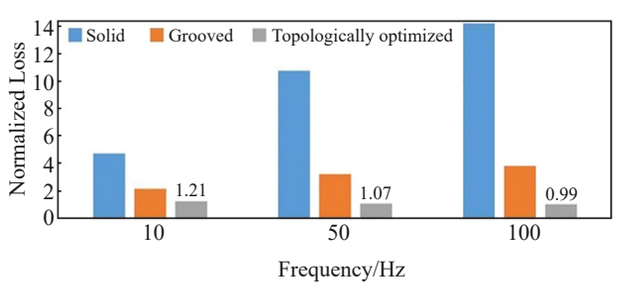

Fig.29 Normalized loss for solid, grooved, and topologically optimized samples[154]

scanning speed at a perpendicular angle to the initial scanning path before applying the next powder layer. Nam et al[162] reported that dual scanning effectively mitigates gaps caused by partial powder melting, achieving a high density of 96% and a corresponding saturation magnetization of 1.22 T. Notably, this approach enhances compositional uniformity and increases the amorphous phase fraction to 47%, leading to a substantial reduction in coercivity and an improvement in magnetic permeability. A novel dual scanning method[163] was also explored, combining a high-energy-density laser beam to achieve high packing density with a subsequent low-energy density laser beam to refine grains before the application of the next powder layer. This technique produced samples with packing density of 94.59%–99.25%, high saturation magnetization of 226.81 A·m^2/kg, and low coercivity of 130 A/m. Zou et al[164] adopted a chessboard scanning strategy, as illustrated in Fig.33, to address brittleness and microcrack issues in iron-based amorphous alloys. This approach effectively reduced

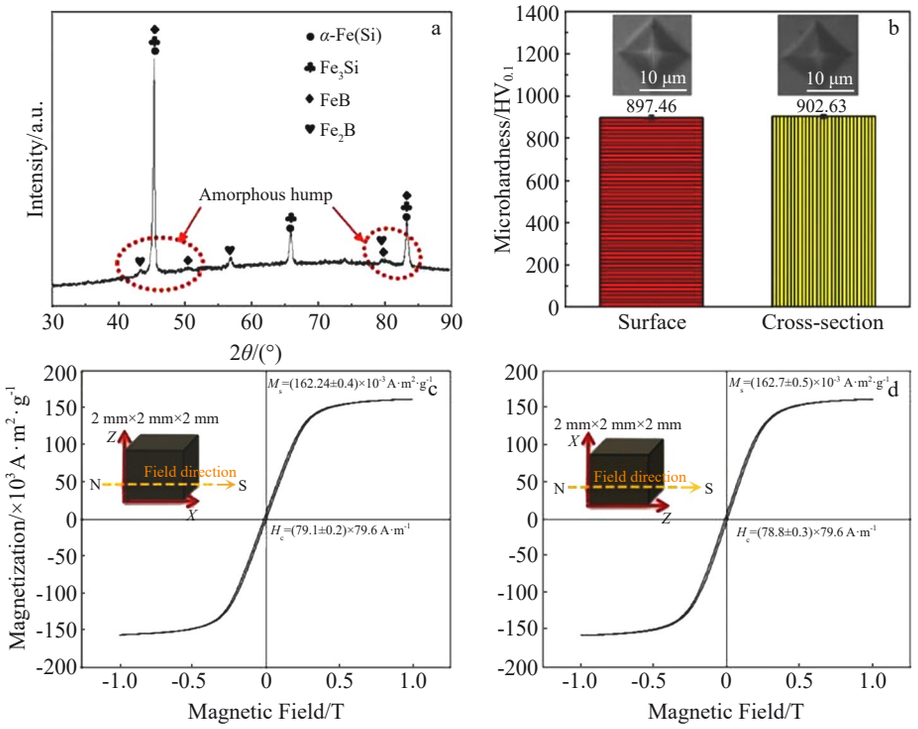

Fig.30 XRD pattern (a), surface and cross-section microhardness results (b), and relationship between magnetization and magnetic field along *X* direction (c) and *Z* direction (d) of SLM-processed FeSi alloys[156]

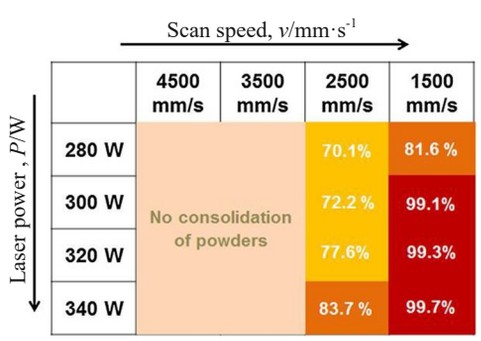

Fig.31 Relative density of SLM samples as a function of laser power and scanning speed[158]

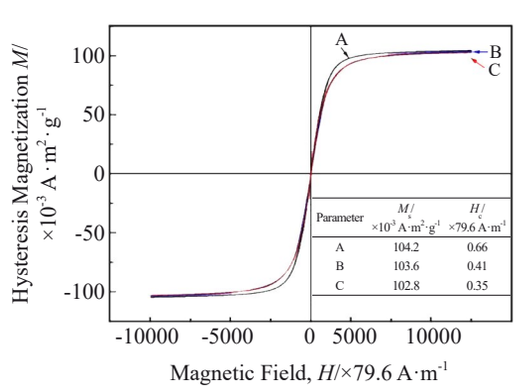

Fig.32 Hysteresis magnetization-magnetic field loops of atomized powders and SLM samples prepared under conditions of v=2500 mm/s and P=340 W as well as v=1500 mm/s and P=340 W[158]

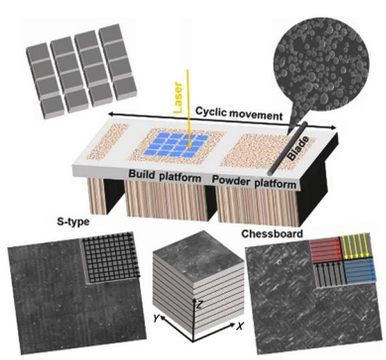

Fig.33 Schematic diagrams of chessboard scanning strategy[164]

residual stress to 168 MPa, which decreased by 29% compared with that produced by conventional scanning strategies. Żrodowski et al[165] proposed a novel two-step melting process, as depicted in Fig.34, which involved initial laser melting followed by a pulse random (P-R) remelting strategy. This method maximized the glass phase fraction and enhanced magnetic properties. Additionally, randomized scanning strategies provided uniform and efficient cooling conditions, further improving material performance.

Numerous studies[166–172] have further investigated the effects of SLM technique on iron-based amorphous soft magnetic alloys. These efforts have provided critical insights into the fabrication of high-performance soft magnetic bulk metallic glasses (BMGs) using SLM, advancing the field of laser manufacturing for BMGs and laying the groundwork for future exploration.

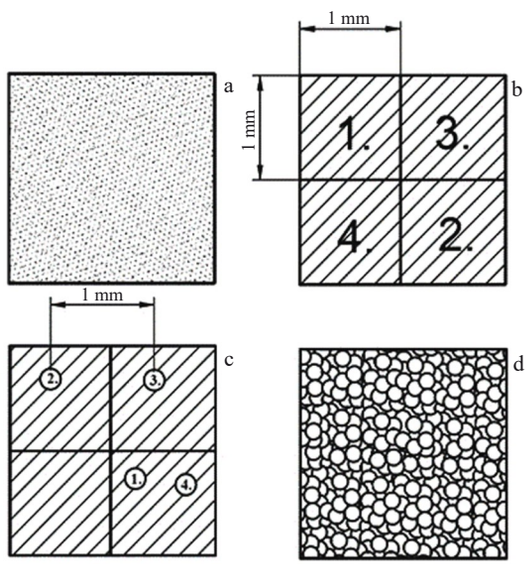

Fig.34 Fabrication schemes for a single layer of metallic glass using novel scanning strategy[165]: (a) loose powder; (b) first melting of the loose powder with the checkerboard strategy; (c) second melting of the previously melted layer using random pulses (the numbers indicate the melting sequence); (d) fully remelted layer after P-R scanning strategy

Beyond soft magnetic alloys, the application of SLM technique for fabricating SMCs has garnered substantial attention[173]. SMCs are prepared by uniformly dispersing magnetic particles within non-magnetic matrices. This configuration minimizes high-frequency eddy current losses while maintaining higher application frequencies. Andrews et al[174] used L-PBF techique to produce NiZnCu ferrite SMCs, achieving superior magnetic permeability, compared with that of traditionally pressed and sintered counterparts using the same powder system and chemical composition.

3 Challenges and Potential Solutions

Recent advancements in SLM technique have markedly improved the manufacturing of soft magnetic alloys, surpassing the restrictions of traditional techniques. SLM offers the design flexibility, facilitating the fabrication of intricate geometries with high material efficiency. Notably, the optimization of process parameters, such as laser power and scanning speed, has led to significant improvements in the microstructure and magnetic properties of soft magnetic alloys, particularly for the materials, such as Fe-Si and Fe-Ni alloys. Furthermore, recent studies have explored the fabrication of various alloys, including amorphous and multi-material composite structures, which exhibit superior soft magnetic properties, such as reduced core losses and improved permeability. Overall, SLM has emerged as a transformative technique in the manufacturing of soft magnetic alloys, offering advanced capabilities for producing complex-shaped high-performance materials. Table 1 summarizes the key

Table 1 Key process parameters and soft magnetic properties of different soft magnetic alloys

Material	Key process parameter	Final material property	Ref.
Fe-3wt%Si	80 W; 0.5 m/s	M_s=0.224 A·m^2·g^{-1}; power loss $P_{50\text{-}1}$ of 18.8 W/kg	[119]
Fe-3wt%Si	200 W; 0.75 m/s; 200 °C (preheating temperature)	μ_{max}=728; H_c=230 A/m	[121]
Fe-9wt%Si	200 W; 0.75 m/s; 800 °C (preheating temperature)	μ_{max}=1 480; H_c=152 A/m	[121]
Fe-6.9wt%Si	70 W; 0.25 m/s; heat treatment of 700 °C/5 h	μ_{max}=5 300; H_c=49 A/m; $P_{50\text{-}1}$=4 W/kg	[126]
Fe-3wt%Si	80 W; 0.5 m/s; heat treatment of 1 000 °C/5 h	μ_{max}=3 370; H_c=92 A/m; $P_{50\text{-}1}$=13.2 W/kg; B_s=1.64 T; B_r=0.763 T	[131]
Fe-6.7wt%Si	235 W; 0.675 m/s; heat treatment of 1 200 °C/1.5 h	μ_{max}=8 361; $P_{50\text{-}1}$=7.7 W/kg	[137]
FeSiB	90 W; 0.1–1.5 m/s	M_s=0.188 6–0.199 0 A·m^2·g^{-1}; H_c=3 486.48–5 810.8 A/m	[140]
FeSiNi	300 W; 1.2 m/s	M_s=0.091 8 A·m^2·g^{-1}; H_c=2 149.2 A/m	[141]
Fe-30%Ni	110 W; 0.4 m/s	M_s=400 A·m^2/kg; H_c=480 A/m	[143]
Fe-80%Ni	60 W; 0.1 m/s	M_s=0.099 A·m^2/kg; H_c=2626.8 A/m	[144]
Fe-50%Ni	150 W; 0.8 m/s	M_s=0.151 A·m^2/kg; H_c=549.24 A/m; initial permeability of 310	[146]
Fe-50%Ni	195 W; 0.8 m/s; heat treatment of 1 200 °C/3 h	H_c=100 A/m; μ_{max}=5 000	[85]
Ni-15Fe-5Mo	200 W; 0.4 m/s; heat treatment of 1 050 °C/3 h	M_s=0.078 A·m^2/g; H_c=119.4 A/m	[116]
Fe-Co	120 W; 0.3 m/s	B_s=2.09T; μ_{max}=503; H_c=1 417 A/m	[150]
Fe-Co	Heat treatment of 820 °C/6 h	B_s=2.38 T; μ_{max}=4 789; H_c=702 A/m	[150]
Fe-Co	Heat treatment of 700 °C/1 h+900 °C/10 h	B_s=2.37 T; μ_{max}=5 008; H_c=450 A/m	[150]
Fe-49Co-2V	200 W; 0.775 m/s	B_r=0.9 T; μ_{max}=307; H_c=1 344 A/m	[151]
Fe-50%Co	120 W; 0.3 m/s; heat treatment of 1 300 K/2 h+1 123 K/4 h	B_{max}=2.39 T; μ_{max}=8 000; H_c=112 A/m	[153]
Fe-49Co-2V	200 W; 0.775 m/s; heat treatmet of 700 °C/2 h + 820 °C/10 h	B_{max}=2.23 T; μ_{max}=13 000; H_c=47 A/m	[154]
FeSiBCrC	90 W; 0.3 m/s	M_s=0.162 A·m^2·g^{-1}; H_c=6 288.4 A/m	[156]
FeSiBPCrMoAl	340 W; 1.5 m/s	M_s=0.104 2 A·m^2·g^{-1}; H_c=52.536 A/m	[158]

findings and progress in the development of soft magnetic alloys through the application of SLM.

Significant progress has been achieved in SLM technique to fabricate soft magnetic alloys. However, numerous challenges remain in industrial applications.

As an emerging AM technique, SLM technique is still developing. The rapid melting and solidification mechanisms introduce complexities in the solidification process, which remains largely exploratory and lacks a robust theoretical foundation. Key printing parameters, such as scanning strategy, powder composition, and powder layer thickness, exert significant influence on the solidification dynamics of the material. These factors lead to intricate microstructural changes, including grain growth and texture evolution, which require further in-depth investigation. In traditional manufacturing, constructing multi-material composite structures, such as layered or core-shell configurations, is effective in enhancing the soft magnetic properties of materials. However, the fabrication of such composite structures through SLM presents substantial challenges. For instance, during the preparation of layered composite structures, ensuring the required microstructure in each layer while maintaining excellent interlayer bonding is critical.

Additionally, the restrictions in material properties represent a significant challenge. The incorporation of non-magnetic materials may lead to a reduction in magnetic characteristics of the composite. Furthermore, the printing of novel soft magnetic materials, such as high entropy alloys (HEAs), remains underdeveloped, which restricts the broader application of this technique. Another critical issue is related to the process defects. Inadequate control over laser energy density can result in defects, such as pores and residual stress, while an uneven distribution of magnetic particles can degrade the printing accuracy. Moreover, SLM process frequently demands intricate and costly post-processing steps, including sintering, heat treatment, and magnetization, all of which further complicate the preparation of soft magnetic alloys.

To address these challenges, several solutions have been proposed. In terms of material optimization, approaches, such as using composite materials, developing HEAs, and enhancing interface bonding, can significantly improve the magnetic properties of the materials. Optimizing laser parameters and incorporating magnetic field-assisted techniques show great promise for enhancing printing quality and particle distribution uniformity. Additionally, optimizing heat treatment and magnetization procedure is crucial for post-processing to further elevate the material performance.

4 Summary and Prospect

1) This article provides a comprehensive review of research on the preparation of various soft magnetic alloys using SLM technique. SLM is a viable manufacturing process for developing SMCs, offering the ability to produce near-net-shaped parts, enhance magnetic performance, and reduce processing costs. Soft magnetic alloys, such as Fe-Si, Fe-Ni, Fe-Co, and amorphous alloys, have been fabricated using SLM technique. The performance of these components is influenced by raw material composition, process parameters, scanning strategies, geometric design, and post-processing methods, all of which regulate the microstructure and thereby determine the final properties.

2) Computer simulation offers a powerful tool for predicting the solidification process, microstructure, and properties of SLM-fabricated soft magnetic alloys. By leveraging simulation, process parameters can be optimized, trial-and-error costs are minimized, and print quality is enhanced. Future research should aim to establish a clear relationship between microstructure and macroscopic magnetic properties by combining simulation and experiment approaches, providing a robust theoretical foundation for material design. Recent advancements in intelligent manufacturing, AI, and big data analytics offer additional opportunities for SLM technique.

3) Furthermore, future research should primarily focus on several key areas. Firstly, the development of novel SMC materials, including high entropy ferrites and magnetic shape memory polymers, will be a critical focus. Moreover, exploring the use of biodegradable or biocompatible materials will be essential to broaden the scope of applications. Secondly, process innovation will play a pivotal role, particularly for the advancement of multi-material gradient printing and ultra-high-resolution printing technologies, both of which are expected to enhance fabrication precision and complexity. Additionally, expanding the application of soft magnetic materials in emerging fields, such as soft robotics, electromagnetic shielding, and renewable energy technologies, shows significant potential. Thirdly, interdisciplinary research will be crucial in advancing SLM technique, especially in areas like finite element modeling, standardization, and online quality control. These all contribute to the optimization of SLM processes and improvement of the production efficiency of soft magnetic alloys.

4) The continued development of SLM for soft magnetic alloy fabrication requires extensive research and interdisciplinary collaboration. Such collaboration will drive multidimensional research and expand the application scope of soft magnetic alloys. Future efforts should focus on not only the materials but also the integration of production processes with intelligent technologies, aiming to achieve efficient, precise, and sustainable manufacturing of soft magnetic alloys.

References

1 Liu Z W. *Metals*[J], 2023, 13(7): 1318

2 Gutfleisch O, Willard M A, Bruck E *et al*. *Advanced Materials*[J], 2011, 23(7): 821

3 Jang S M, Seo H J, Park Y S *et al*. *IEEE Transactions on Magnetics*[J], 2012, 48(11): 2933

4 Zhao W, Lipo T A, Kwon B I. *IEEE Transactions on Magnetics*[J], 2014, 50(11): 1

5 Li Y, Li J, Li W *et al*. *Smart Materials and Structures*[J], 2014, 23(12): 123001

6 Hojjati-Najafabadi A, Mansoorianfar M, Liang T *et al*. *Science of the Total Environment*[J], 2022, 824: 153844

7 Wang H, Zhu Z, Jin H *et al*. *Journal of Alloys and Compounds*[J], 2022, 922: 166219

8 Peng Z, Zhai Z, Yang R *et al*. *Materials Today Physics*[J], 2024, 45: 101467

9 He J, Yuan H, Nie M *et al*. *Materials Today Electronics*[J], 2023, 6: 100066

10 Goodall A D, Uramowski J, Sinclair C W *et al*. *Additive Manufacturing Letters*[J], 2023, 7: 100179

11 You J, Yu H, Liang H *et al*. *Chinese Journal of Aeronautics*[J], 2022, 35(9): 379

12 Yu J, Feng H, Jiang S *et al*. *Materials Characterization*[J], 2023, 204: 113223

13 Zhang L, Wang Y, Ke Y *et al*. *Separation and Purification Technology*[J], 2024, 328: 125090

14 Rodionov S A, Kulikova D P, Pomozov A R *et al*. *Optical Materials*[J], 2023, 145: 114484

15 Shokrollahi H, Janghorban K. *Journal of Materials Processing Technology*[J], 2007, 189(1–3): 1

16 Kustas A B, Susan D F, Monson T. *The Journal of the Minerals, Metals & Materials Society*[J], 2022, 74(4): 1306

17 Silveyra J M, Ferrara E, Huber D L *et al*. *Science*[J], 2018, 362(6413): eaao0195

18 Goodall A D, Chechik L, Mitchell R L *et al*. *Additive Manufacturing*[J], 2023, 70: 103555

19 Ansari M H, Iacovacci V, Pane S *et al*. *Advanced Functional Materials*[J], 2023, 33(15): 2211918

20 Sai R B, Paul A K, Kulkarni S V. *Journal of Magnetism and Magnetic Materials*[J], 2021, 537: 168210

21 Wang F H, You C Y, Tian N *et al*. *Journal of Alloys and Compounds*[J], 2024, 990: 174486

22 Jian G, Zhou D, Yang J *et al*. *Journal of Magnetism and Magnetic Materials*[J], 2012, 324(24): 4179

23 Yang Y W, Wang Y L, Yang L *et al*. *Rare Metal Materials and Engineering*[J], 2022, 51(8): 2727

24 Zhang J, Zhang C, Zhang X *et al*. *Journal of Alloys and Compounds*[J], 2021, 866: 158991

25 Du J C, Li X F, Jiao P Y *et al*. *Rare Metal Materials and Engineering*[J], 2024, 53(8): 2144

26 Hsiang H I, Chen C H, Chen C C. *Journal of Materials Science: Materials in Electronics*[J], 2021, 32(11): 14584

27 Li W C, Wang C, Ying Y *et al*. *Journal of Electronic Materials*[J], 2021, 50(8): 4812

28 Ma J D, Qin M, Zhang L *et al*. *Journal of Magnetism and Magnetic Materials*[J], 2013, 329: 24

29 Zhang Y, Ma R, Feng S *et al*. *Journal of Magnetism and Magnetic Materials*[J], 2020, 497: 165982

30 Ma R, Yu P. *Materials Research Bulletin*[J], 2021, 139: 111256

31 Ma R, Chang L, Dong Y *et al*. *Powder Technology*[J], 2022, 397: 116986

32 Bures R, Faberova M, Bircakova Z *et al*. *Powder Technology*[J], 2023, 421: 118434

33 Huang H, Zhang R, Sun H *et al*. *Journal of Alloys and Compounds*[J], 2023, 947: 169460

34 Pan Y, Peng J, Qian L *et al*. *Materials Research Express*[J], 2020, 7(1): 016115

35 Maciaszek R, Kollár P, Birčáková Z *et al*. *Journal of Materials Science*[J], 2024, 59(26): 11781

36 Lu L L, Yan Q, Chen F G *et al*. *Materials Today Communications*[J], 2024, 38: 108407

37 Thomas S V, Willard M A, Martone A *et al*. *Physica Status Solidi* (*a*)[J], 2020, 217: 1900680

38 Srinivas M, Majumdar B, Phanikumar G *et al*. *Metallurgical and Materials Transactions B*[J], 2011, 42(2): 370

39 Wang R, He Y H, Kong H *et al*. *Ceramics International*[J], 2022, 48(20): 29854

40 Kocsis B, Fekete I, Varga L K. *Journal of Magnetism and Magnetic Materials*[J], 2020, 501: 166425

41 Belcher C H, Zheng B, MacDonald B E *et al*. *Journal of Materials Science*[J], 2022, 57(9): 5518

42 Srivastava Y, Srivastava S. *Journal of Magnetism and Magnetic Materials*[J], 2017, 423: 267

43 Astacio R, Ternero F, Cintas J *et al*. *Metals*[J], 2021, 11(6): 994

44 Kang S, Lee S. *Metals*[J], 2024, 14(7): 815

45 Wei X, Jin M L, Yang H *et al*. *Journal of Advanced Ceramics*[J], 2022, 11(5): 665

46 Bollero A, Rial J, Villanueva M *et al*. *ACS Sustainable Chemistry & Engineering*[J], 2017, 5(4): 3243

47 Yin H X, Qu M, Zhang H Y *et al*. *Technology|Architecture+Design*[J], 2018, 2(1): 94

48 Wang J, Zhang Y, Aghda N H *et al*. *Advanced Drug Delivery Reviews*[J], 2021, 174: 294

49 Lee J Y, An J, Chua C K. *Applied Materials Today*[J], 2017, 7: 120

50 Gao W, Zhang Y, Ramanujan D *et al*. *Computer-Aided Design*[J], 2015, 69: 65

51 Mahmood A, Akram T, Chen H *et al*. *Polymers*[J], 2022, 14(21): 4698

52 Yang E, Miao S D, Zhong J *et al*. *Polymers Reviews*[J], 2018, 58(4): 668

53 Jordan R S, Wang Y. *Journal of Polymer Science Part B: Polymer Physics*[J], 2019, 57(23): 1592

54 Liu F, Wang X H. *Polymers*[J], 2020, 12(8): 1765

55 Yuk H, Lu B, Lin S *et al*. *Nature Communications*[J], 2020, 11(1): 1604

56 Lin Xin, Huang Weidong. *Materials China*[J], 2015, 34(9): 21 (in Chinese)

57 Liu B, Liu S, Devaraj V *et al*. *Nature Communications*[J], 2023, 14(1): 4920

58 Guo X, Huang H L, Zhu M *et al*. *Materials Today*[J], 2023, 66: 92

59 Abdullah T, Qurban R O, Bolarinwa S O *et al*. *Frontiers in Bioengineering and Biotechnology*[J], 2020, 8: 568186

60 Panwisawas C, Tang Y T, Reed R C. *Nature Communications*[J], 2020, 11(1): 2327

61 Wang Y, Bu Y, Wang X. *Journal of the European Ceramic Society*[J], 2024, 44(14): 116653

62 He Junhong, Wu Jiamin, Chen Annan *et al*. *Materials China*[J], 2020, 39(5): 337 (in Chinese)

63 Chen Z, Li Z, Li J *et al*. *Journal of the European Ceramic Society*[J], 2019, 39(4): 661

64 Bose S, Akdogan E K, Balla V K *et al*. *Journal of the American Ceramic Society*[J], 2024, 107(12): 7879

65 Chen Z, Sun X, Shang Y *et al*. *Journal of Advanced Ceramics*[J], 2021, 10(2): 195

66 Bodkhe S, Vigo L, Zhu S *et al*. *Additive Manufacturing*[J], 2020, 35: 101290

67 Ma T, Zhang Y, Ruan K *et al*. *InfoMat*[J], 2024, 6(6): e12568

68 He X, Ding Y, Lei Z *et al*. *Additive Manufacturing*[J], 2021, 40: 101921

69 Archez J, Texier-Mandoki N, Bourbon X *et al*. *Journal of Building Engineering*[J], 2021, 34: 101894

70 Liu Z, Zhou W, Lu Y *et al*. *Materials Letters*[J], 2018, 225: 85

71 Pourrahimi S, Hof L A. *Advanced Engineering Materials*[J], 2024, 26(10): 2301511

72 Leary M, Mazur M, Watson M *et al*. *The International Journal of Advanced Manufacturing Technology*[J], 2019, 105(1–4): 1

73 McNeil J L, Sisco K, Frederick C *et al*. *Metallurgical and Materials Transactions A*[J], 2020, 51(12): 6528

74 Bruggeman K, Klingbeil N, Palazotto A. *Journal of Materials Engineering and Performance*[J], 2024, 33(8): 4088

75 Jian B C, Demoly F, Zhang Y C *et al*. *Engineering*[J], 2022, 12: 70

76 Li H, Yin Y, Xiang Y *et al*. *Biomed Mater*[J], 2020, 15(4): 5004

77 Gul J Z, Sajid M, Rehman M M *et al*. *Sci Technol Adv Mater*[J], 2018, 19(1): 243

78 Li R, Yuan S, Zhang W *et al*. *ACS Appl Mater Interfaces*[J], 2019, 11(43): 40564

79 Dermanaki F R, Dubé M. *Advanced Engineering Materials*[J], 2017, 20(2): 1700539

80 Guo S Z, Qiu K, Meng F *et al*. *Adv Mater*[J], 2017, 29(27): 1700539

81 Zhao J X, Zhang H Y, Huang Y *et al*. *Adv Sci*[J], 2018, 5(11): 1801114

82 Park J, Kim J K, Kim D S *et al*. *Sensors and Actuators B: Chemical*[J], 2019, 280: 201

83 Pham T, Kwon P, Foster S. *Energies*[J], 2021, 14(2): 283

84 Périgo E A, Jacimovic J, García Ferré F *et al*. *Additive Manufacturing*[J], 2019, 30: 100870

85 Mazeeva A K, Staritsyn M V, Bobyr V V *et al*. *Journal of Alloys and Compounds*[J], 2020, 814: 152315

86 Yang S, Tang Y, Zhao Y F. *Journal of Manufacturing Processes*[J], 2015, 20: 444

87 Lamichhane T N, Sethuraman L, Dalagan A *et al*. *Materials Today Physics*[J], 2020, 15: 100255

88 Atzeni E, Salmi A. *The International Journal of Advanced Manufacturing Technology*[J], 2012, 62(9–12): 1147

89 Gao B W, Zhao H J, Peng L Q *et al*. *Micromachines*[J], 2022, 14(1): 57

90 Yap C Y, Chua C K, Dong Z L *et al*. *Applied Physics Reviews*[J], 2015, 2(4): 041101

91 Rodriguez-Vargas B R, Stornelli G, Folgarait P *et al*. *Materials*[J], 2023, 16(16): 5610

92 Bremen S, Meiners W, Diatlov A. *Laser Technik Journal*[J], 2012, 9(2): 33

93 Zhang D Y, Wang W D, Guo Y W *et al*. *Journal of Materials Processing Technology*[J], 2019, 268: 25

94 Wilkes J, Hagedorn Y C, Meiners W *et al*. *Rapid Prototyping Journal*[J], 2013, 19(1): 51

95 Marcu T, Todea M, Gligor I *et al*. *Applied Surface Science*[J], 2012, 258(7): 3276

96 Irrinki H, Dexter M, Barmore B *et al*. *The Journal of the Minerals, Metals & Materials Society*[J], 2016, 68(3): 860

97 Irrinki H, Harper T, Badwe S *et al*. *Progress in Additive Manufacturing*[J], 2018, 3(1–2): 39

98 Zhang J Y, Gu D F, Yang Y *et al*. *Engineering*[J], 2019, 5(4): 736

99 Ng C C, Savalani M M, Lau M L *et al*. *Applied Surface Science*[J], 2011, 257(17): 7447

100 Attar H, Prashanth K G, Zhang L C *et al*. *Journal of Materials Science & Technology*[J], 2015, 31(10): 1001

101 Stornelli G, Vargas B R R, Folgarait P *et al*. *MRS Advances*[J], 2023, 8(21): 1195

102 Zhang L C, Attar H. *Advanced Engineering Materials*[J], 2015, 18(4): 463

103 Xie M, Li F, Zhou S *et al*. *Journal of Materials Research and Technology*[J], 2023, 26: 2759

104 Hemmati M, Modabberifar M, Taheri M *et al*. *Materialwissenschaft und Werkstofftechnik*[J], 2023, 54(11): 1330

105 Andreiev A, Hoyer K P, Dula D *et al*. *Journal of Materials Processing Technology*[J], 2021, 296: 117183

106 Sajjadi M A, Modabberifar M, Taheri M *et al*. *Journal of Magnetism and Magnetic Materials*[J], 2024, 596: 171924

107 Yasa E, Deckers J, Kruth J P. *Rapid Prototyping Journal*[J], 2011, 17(5): 312

108 Attar H, Calin M, Zhang L C *et al*. *Materials Science and Engineering A*[J], 2014, 593: 170

109 Do D K, Li P. *Virtual and Physical Prototyping*[J], 2016, 11(1): 41

110 Yadroitsev I, Bertrand P, Smurov I. *Applied Surface Science*[J], 2007, 253(19): 8064

111 Yadroitsev I, Yadroitsava I, Bertrand P *et al*. *Rapid Prototyping*

Journal[J], 2012, 18(3): 201

112 Haftlang F, Kim E S, Kim H S. *Journal of Materials Processing Technology*[J], 2022, 309: 117733

113 Geiger F, Kunze K, Etter T. *Materials Science and Engineering A*[J], 2016, 661: 240

114 Xie J W, Fox P, O'Neill W *et al*. *Journal of Materials Processing Technology*[J], 2005, 170(3): 516

115 Yang J X, Zhu Q, Wang Z K *et al*. *Materials Characterization*[J], 2023, 197: 112672

116 Lv X D, Wen B, Du J H. *Rare Metal Materials and Engineering*[J], 2019, 48(5): 1386

117 Kang N, Li Q, Mansori M E *et al*. *Chinese Journal of Mechanical Engineering: Additive Manufacturing Frontiers*[J], 2022, 1(4): 100054

118 Szczepański Ł, Bambach M, Jensch F *et al*. *Materials & Design*[J], 2021, 210: 110112

119 Gao S H, Liao H L, Yan X C *et al*. *Journal of Magnetism and Magnetic Materials*[J], 2023, 580: 170907

120 Zhong K J, Chang T W, Lee W H *et al*. *AIP Advances*[J], 2019, 9(3): 035317

121 Backes C, Kahlert M, Vollmer M *et al*. *Journal of Materials Research and Technology*[J], 2024, 29: 1691

122 Ji M, Shim H J, Kim J H *et al*. *Powder Metallurgy*[J], 2023, 66(5): 602

123 Stella M, Faba A, Fulginei F R *et al*. *Journal of Magnetism and Magnetic Materials*[J], 2024, 591: 171752

124 Teh W H, Tan L P, Chen S *et al*. *Journal of Alloys and Compounds*[J], 2024, 983: 173829

125 Garibaldi M, Ashcroft I, Simonelli M *et al*. *Acta Materialia*[J], 2016, 110: 207

126 Garibaldi M, Ashcroft I, Hillier N *et al*. *Materials Characterization*[J], 2018, 143: 144

127 Hwang J Y, Jung H Y. *Progress in Additive Manufacturing*[J], 2024, 10: 959

128 Shen X J, Sheng H, He Y J *et al*. *Materials & Design*[J], 2023, 234: 112343

129 Andreiev A, Hoyer K P, Hengsbach F *et al*. *Journal of Materials Processing Technology*[J], 2023, 317: 117991

130 Faba A, Fulginei F R, Antonio S Q *et al*. *IEEE Transactions on Industrial Electronics*[J], 2024, 71(3): 2188

131 Gao S H, Liao H L, Yan X C *et al*. *Journal of Alloys and Compounds*[J], 2023, 951: 169840

132 Garibaldi M, Ashcroft I, Lemke J N *et al*. *Scripta Materialia*[J], 2018, 142: 121

133 Haines M P, List F, Carver K *et al*. *Additive Manufacturing*[J], 2022, 50: 102578

134 Plotkowski A, Pries J, List F *et al*. *Additive Manufacturing*[J], 2019, 29: 100781

135 Koo B, Jang M S, Nam Y G *et al*. *Applied Surface Science*[J], 2021, 553: 149510

136 Lyrio M S, Aota L S, Sandim M J R *et al*. *Journal of Materials Science*[J], 2024, 59(9): 4019

137 Ouyang G, Chen X, Liang Y *et al*. *Journal of Magnetism and Magnetic Materials*[J], 2019, 481: 234

138 Goll D, Schuller D, Martinek G *et al*. *Additive Manufacturing*[J], 2019, 27: 428

139 Macknojia A Z, Tran J V, McKinstry M P *et al*. *Materials & Design*[J], 2024, 241: 112883

140 Alleg S, Drablia R, Fenineche N. *Journal of Superconductivity and Novel Magnetism*[J], 2018, 31(11): 3565

141 Kang N, El Mansori M, Guittonneau F *et al*. *Applied Surface Science*[J], 2018, 455: 736

142 Mandal S, Kumar M, Sengupta P *et al*. *ACS Omega*[J], 2024, 9(13): 15650

143 Zhang B, Fenineche N E, Liao H *et al*. *Journal of Materials Science & Technology*[J], 2013, 29(8): 757

144 Zhang B, Fenineche N E, Liao H *et al*. *Journal of Magnetism and Magnetic Materials*[J], 2013, 336: 49

145 Shishkovsky I, Saphronov V. *Materials Letters*[J], 2016, 171: 208

146 Liu H, Wang S, Ma Y *et al*. *Journal of Magnetism and Magnetic Materials*[J], 2023, 580: 170962

147 Zou J, Gaber Y, Voulazeris G *et al*. *Acta Materialia*[J], 2018, 158: 230

148 Babuska T F, Wilson M A, Johnson K L *et al*. *Acta Materialia*[J], 2019, 180: 149

149 Babuska T F, Johnson K L, Verdonik T *et al*. *Additive Manufacturing*[J], 2020, 34: 101187

150 Li S, Lau K B, Wuu D *et al*. *Additive Manufacturing*[J], 2021, 47: 102291

151 Riipinen T, Metsä-Kortelainen S, Lindroos T *et al*. *Rapid Prototyping Journal*[J], 2019, 25(4): 699

152 Sourmail T. *Progress in Materials Science*[J], 2005, 50(7): 816

153 Liogas K A, Lau K B, Wang Z *et al*. *Additive Manufacturing*[J], 2023, 67: 103499

154 Lindroos T, Riipinen T, Metsä-Kortelainen S *et al*. *Journal of Magnetism and Magnetic Materials*[J], 2022, 563: 169977

155 Everhart W, Newkirk J. *Applied Sciences*[J], 2019, 9(18): 3701

156 Gao S, Yan X, Chang C *et al*. *Materials Letters*[J], 2021, 290: 129469

157 Sufiiarov V, Erutin D, Kantyukov A *et al*. *Materials*[J], 2022, 15(12): 4121

158 Jung H Y, Choi S J, Prashanth K G *et al*. *Materials & Design*[J], 2015, 86: 703

159 Özden M G, Freeman F S H B, Morley N A. *Advanced Engineering Materials*[J], 2023, 25(19): 2300597

160 Rodríguez-Sánchez M, Sadanand S, Ghavimi A *et al*. *Materialia*[J], 2024, 35: 102111

161 Maurya H S, Vikram R J, Kumar R *et al*. *Micron*[J], 2024, 180: 103613

162 Nam Y G, Koo B, Chang M S *et al*. *Materials Letters*[J], 2020, 261: 127068

163 Özden M G, Morley N A. *Advanced Engineering Materials*[J], 2023, 25(22): 2300700
164 Zou Y M, Wu Y S, Li K F *et al*. *Materials Letters*[J], 2020, 272: 127824
165 Żrodowski Ł, Wysocki B, Wróblewski R *et al*. *Journal of Alloys and Compounds*[J], 2019, 771: 769
166 Luo N, Scheitler C, Ciftci N *et al*. *Materials Characterization*[J], 2020, 162: 110206
167 Pauly S, Löber L, Petters R *et al*. *Materials Today*[J], 2013, 16(1–2): 37
168 Xing W, Ouyang D, Li N *et al*. *Intermetallics*[J], 2018, 103: 101
169 Jiang Q, Zhang P L, Tan J *et al*. *Journal of Alloys and Compounds*[J], 2022, 894: 162525
170 Zou Y, Qiu Z, Tan C *et al*. *Journal of Non-crystalline Solids*[J], 2020, 538: 120046
171 Nong X D, Zhou X L, Ren Y X. *Optics & Laser Technology*[J], 2019, 109: 20
172 Özden M G, Morley N A. *Journal of Alloys and Compounds*[J], 2023, 960: 170644
173 Benack N C, Wang T, Matthews K *et al*. *Microscopy and Microanalysis*[J], 2018, 24(S1): 1066
174 Andrews C E, Chatham M P, Dorman S F *et al*. *Journal of Materials Research*[J], 2021, 36(18): 3579

激光选区熔化-3D打印软磁合金：工艺、性能和前景

刘炳旭，游才印，王凤辉，田　娜，刘和光，张　静，朱孝培
(西安理工大学 材料科学与工程学院，陕西 西安 710048)

摘　要：软磁合金因其具有高饱和磁感应强度、低矫顽力和高磁导率等优点，被广泛应用于各种电力电子设备中。在某些应用中，越来越需要复杂形状的组件来提高性能。增材制造技术，特别是选区激光熔化（SLM）技术，已经成为制造复杂形状软磁元件的有效方法。SLM是一种基于激光的增材制造技术，采用高功率密度激光在粉末床内熔化和融合金属粉末。这种方法可以实现快速原型制作、精确的几何控制和多材料设计的集成。本文重点介绍了SLM技术在Fe-Si、Fe-Ni、Fe-Co和非晶合金体系等软磁合金研究中的应用进展。此外，还探讨了SLM在制造过程中的实施方案，并评估了基于SLM制备技术的软磁合金研发相关的机遇和挑战。

关键词：增材制造；选区激光熔化；软磁合金；磁性

作者简介：刘炳旭，2000年生，男，硕士，西安理工大学材料科学与工程学院，陕西 西安 710048，E-mail：3234237284@qq.com